JIMMA UNIVERSITY

SCHOOL OF GRADUATE STUDIES

JIMMA INSTITUTE OF TECHNOLOGY

FACULTY OF CIVIL AND ENVIRONMENTAL ENGINEERING

STRUCTURAL ENGINEERING

Moment Redistribution Behavior of Steel Fiber Reinforced Concrete Continuous Beams

A Thesis Submitted to the School of Graduate Studies of Jimma University in Partial Fulfilment of the Requirements for the Degree of Master of Science in Structural Engineering.

By

Yohannes Werkina

November 2018

Jimma, Ethiopia

JIMMA UNIVERSITY

SCHOOL OF GRADUATE STUDIES

JIMMA INSTITUTE OF TECHNOLOGY

FACULTY OF CIVIL AND ENVIRONMENTAL ENGINEERING

STRUCTURAL ENGINEERING

Moment Redistribution Behavior of Steel Fiber Reinforced Concrete Continuous Beams

A Thesis Submitted to the School of Graduate Studies of Jimma University in Partial Fulfilment of the Requirements for the Degree of Master of Science in Structural Engineering.

By

Yohannes Werkina

Advisor: Elmer C. Agon (Ass. Prof.)

Co-advisor: Engr. Vinoth Kumar (Ass. Prof.)

November 2018

Jimma, Ethiopia

DECLARATION

By submitting this thesis, I declare that the entirety of the work contained therein is my own, original work, that I am the owner of the copyright thereof (unless to the extent explicitly otherwise stated) and that I have not previously in its entirety or in part submitted it for obtaining any qualification. All secondary sources referred to in this work have been duly acknowledged.

Name: Yohannes Werkina

Signature:

Place: Jimma University, Jimma Institute of Technology

Date of Submission: November 2018

Elmer C. Agon (Ass. Prof.)	_____	_____
Advisor	Signature	Date

Vinoth Kumar (Ass. Prof.)	_____	_____
Co-Advisor	Signature	Date

ABSTRACT

The redistribution of moment has been confirmed in reinforced concrete structure by experimental investigations. It is also a fact that reinforced concrete structures have comparatively lower capacity to rotate than steel structures. Yet, this phenomenon is drawing the attention of the designers. Presently, design codes of most of countries allow the redistribution up to maximum limit. The addition of steel fibers will enhance the redistribution of moment forming ductile section.

The study characterized the moment redistribution behavior of a steel fiber reinforced concrete (SFRC) continuous beam subjected to five point bending test modelled in FEA using constitutive material model. The compression behavior was obtained using uniaxial compression strength tests while the tensile behavior was obtained using splitting strength test analysis performed according to flexural test results. These properties were utilized to derive a theoretical moment-curvature relation for each SFRC member which supplied the basis for the characterized moment-rotation behavior and the finite element analyses (FEA) performed on the continuous beam. The laboratory tests for compressive and splitting tensile strength of SFRC were conducted for volume of steel fibers, 0%, 0.5%, 0.75% and 1.5%. From the tests results it was observed that the compressive strength increased by 26.8% for 0.5% SFRC, 30.7% for 0.75% SFRC and reduced by 5.3% for 1.5% SFRC. The splitting tensile strength increased by 11.2% for 0.5%, 5.8% for 0.75% and 2.5% for 1.5% SFRC. Increment of peak strain was also confirmed. The ductility of the member was increased 1.59 times, 2.41 times and 3.25 for 0.5%, 0.75% and 1.5% SFRC member respectively, compared to that of the 0 % SFRC member's rotation capability. Section moment capacity was also enhanced by Increasing steel fibers volume.

The development of the moment redistribution was accompanied by the rotation of the plastic hinges at the critical sections in the beam. The amount of moment redistribution of SFRC reduced as volume of steel fiber increased. So utilizing permissible moment redistribution for SFRC as prescribed by design standards needs further study.

Key Words: SFRC, Moment Redistribution, Continuous Beam, FEA

ACKNOWLEDGEMENT

First I would like to thank my Advisors, Elmer C. Agon and Vinoth Kumar, for their advice over this research proposal and also for their academic courses I had with them for the last semesters.

I gratefully acknowledge the bodies which funded this research. These are: Jimma University and Ethiopian Road Authority Sponsorship.

In particular, I would like to thank those who helped me in giving information on experimental activities and thesis writing

Lastly, Jimma Institute of Technology Structural Engineering Chair senior staffs for their valuable advice is fully acknowledged.

TABLE OF CONTENTS

LIST OF TABLES

LIST OF FIGURES

ACRONYMS

FEA/M	Finite Element Analysis/Model
FRC	Fiber Reinforced Concrete
SFRC	Steel Fiber Reinforced Concrete
SF	Steel fiber
ES EN	Ethiopian Standard European Norm
ACI	American Concrete Institute
MR	Moment Redistribution
V_f	Volume fraction of steel fiber
$N.A$	Neutral axis
$M-\varphi$	Moment-curvature
$M-\theta$	Moment-rotation
f_{ck}	Compressive strength of concrete
f_y	Yielding stress of steel
E	Modulus of elasticity
M_e	Elastic Moment
M_y	Yielding Moment
M_{cr}	Cracking Moment
M_{red}	Redistributed moment
B	Width of the beam section
D	Depth of the beam section
d	Effective depth
L	Span length
I	Area moments of inertia
h_1	Top position of the neutral axis
h_2	Bottom position of the neutral axis
l_b	Equivalent plastic hinge length
C	Compression force
T	Tensile force

β	Fiber index
δ	Displacement
ε	Strain
φ_y, ϕ_y	Yield Curvature
φ_u, ϕ_u	Ultimate Curvature
γ	Stress mobilization factor
θ	Rotation
θ_p	Plastic rotation
ρ	Reinforcement ration
σ	Stress
ω	Reinforcement index
$\tilde{\varepsilon}_c^{in}$	Inelastic strain

CHAPTER ONE

INTRODUCTION

1.1 Background

Steel fibre reinforced concrete (SFRC) is the most prominent fibre reinforced concrete composite that was engineered to enhance the material's post-cracking behavior. In certain situations it is utilized to replace conventional reinforcement and considered to be more cost-efficient (Möhr, 2012).

The SFRC is a composite material made of cement, fine and coarse aggregates and discontinuous discrete steel fibers. In tension SFRC fails only after the steel fiber breaks or pulled out of the cement matrix. The composite nature of SFRC is responsible for its properties in freshly mixed and hardened state (Dahake & Charkha, 2016).

The SFRC possess many excellent dynamic performances such as high resistance to explosion and penetration as compared to traditional concrete. When used in structural applications, SFRC should only be used in a supplementary role to inhibit cracking, to improve resistance to impact or dynamic loading and resist material disintegration (Dahake & Charkha, 2016). The mechanical properties of SFRC are influenced by the type of fiber, aspect ratio, and volume fraction of fibers and the size of the aggregates. One of the most important properties of SFRC is its ability to transfer stresses across a cracked section which increases toughness of concrete in hardened state (Dahake & Charkha, 2016).

Recently, as the demand for high strength concrete has increased, the structural behavior of reinforced concrete has become more brittle. In order to reduce this side effect, steel fiber-reinforced concrete (SFRC) has arisen as a viable method to attain ductility not only during post-cracking behavior under tension, but also during post-peak softening behavior under compression (Lee, et al., 2015).

Considerable research had been carried out to evaluate mechanical properties such as tensile, compressive, flexural, and impact strength of steel fiber reinforced cement composites.

According to Singh (2017) the contribution of fibers is most apparent in the post-peak region in the case of the SFRC, where the response is described by a relatively less steep decaying stress-strain response. Once the matrix cracks under induced tension, the debonding and pulling out of the fibers from the concrete dissipates energy, thereby, leading to a substantial increase in the post-cracking characteristics (Singh, 2017).

The basic idea for moment redistribution in continuous reinforced concrete beams as Hassan & Reza (2013) study is that the demand rotation required for the development of plastic hinges at the ends and middle of the spans should be lower than the rotational capacity of the plastic hinge or hinges that yield first. The rotational capacity in members could easily be transfer red to section curvature capacity using the concept of plastic hinge length (Hassan & Reza, 2013).

1.2 Statement of the Problem

The allowable amount of moment redistribution is prescribed in structural design codes such as ES EN 2015 and ACI for conventional Reinforced Concrete design, but has not been considered for SFRCs. This phenomenon could have a major influence in the structural design process for SFRC and a situation when conventional steel is implemented in conjunction with steel fibers.

The addition of steel fibers to reinforced concrete enhance ductility, plastic hinge formation prior to failure in continuous flexural members (beams) to redistribute the moments by forming rotations around boundary conditions. So using the advantages of moment redistribution behavior of continuous beams the designer can design the member beyond elastic region to minimize the reinforcement needed.

While extensive research is being conducted on SFRC material, the utilization of SFRC in the construction industry has been very limited due to insufficient details on the design procedures and an absence of a code allowing the use of tensile contribution in SFRC elements. The emerging development of adopting steel fibers in construction industries/structures needs new knowledge about the behavior and strength of the fibers. Many researchers carried out laboratory test and Finite element modeling techniques to examine the effect and behavior of SFRC in compressive and tensile strength of the

structure. But the behavior of moment redistribution of SFRC members is not widely researched, so that this study is carried out to fill the existing gap.

1.3 Research Questions

The research questions for this study were:

1. What are the effects of steel fibers addition on compressive and tensile strength of SFRC?
2. How moment-curvature response and moment-rotation response of SFRC Continuous beam is affected?
3. Is that possible to utilize the prescribed moment redistribution values in current design codes of ES EN 2015 and ACI for the design of steel fibre reinforced concrete structures?

1.4 Objectives of the Study

1.4.1 General objective

The general objective of the study was to investigate the Moment Redistribution behavior of Steel Fiber Reinforced Concrete continuous beams.

1.4.2 Specific Objectives

- To check the compressive and tensile strength of SFRC
- To determine the moment – curvature, to examine plastic hinge length and rotation, and to investigate moment – rotation relations for continuous SFRC beam
- To formulate and analyze SFRC continuous beam in software (FEM) modeling

1.5 Significance of the Study

The significance of the study was to clearly specify the behavior of SFRC moment redistribution behavior of continuous beam. This research was studied for understanding of material properties and developing design models in order to develop a codified

approach for the utilization of SFRC for moment redistribution. It also furthermore provided guidance to the designers and code writers for SFRC material on the appropriateness of using steel fibers in different situations. Knowing the behavior of SFRC to accommodate moment redistribution, the end user of the study (future researchers, institutions and students) will use SFRC as material in design of members and maintenance of structures.

1.6 Scope and Limitation of the Study

Since the study of steel fibers effect on reinforce concrete member in recent years includes adverse analysis and experimental investigation. Many researchers studied the flexural strength, shear strength behavior and moment redistribution. This study predicted the amount and behavior of moment redistributed for varying steel fiber volume for 0%, 0.5%, 0.75% and 1.5% steel fibers after result obtained from experimental test (Compressive and Tensile strength of SRFC). Since casting the continuous SFRC beam in Laboratory is difficult and not available, the study used model in FEA software, ABAQUS using constitutive material model.

The study was limited to investigate only theoretical moment- curvature response, moment–rotation response and amount of moment redistribution of two span SRFC beam subjected to concentrated loading using five point bending.

CHAPTER TWO

RELATED LITERATURE REVIEW

2.1 Fiber Reinforced Concrete (FRC)

Fiber Reinforced Concrete (FRC) is a composite material made primarily from hydraulic cements, aggregates and discrete reinforcing fibers. Fiber incorporation in concrete, mortar and cement paste enhances many of the engineering properties of these materials such as fracture toughness, flexural strength, resistance to fatigue, impact, thermal shock etc., and guidelines which fully utilizes the advantages of FRC. (Dahake & Charkha, 2016)

The fiber reinforced concrete is produced using different types of fibers. The fibers are mainly classified in two groups as metallic and non-metallic fibers. (Dahake & Charkha, 2016)

2.1.1 Compressive and Tensile Behavior of FRC Materials

Typical compressive stress–strain responses for different fiber reinforced concrete are done and presented as follows in Figure 2.1 by researchers, Padmarajaiah, et al. (2002) and Tejchman, et al. (2010).

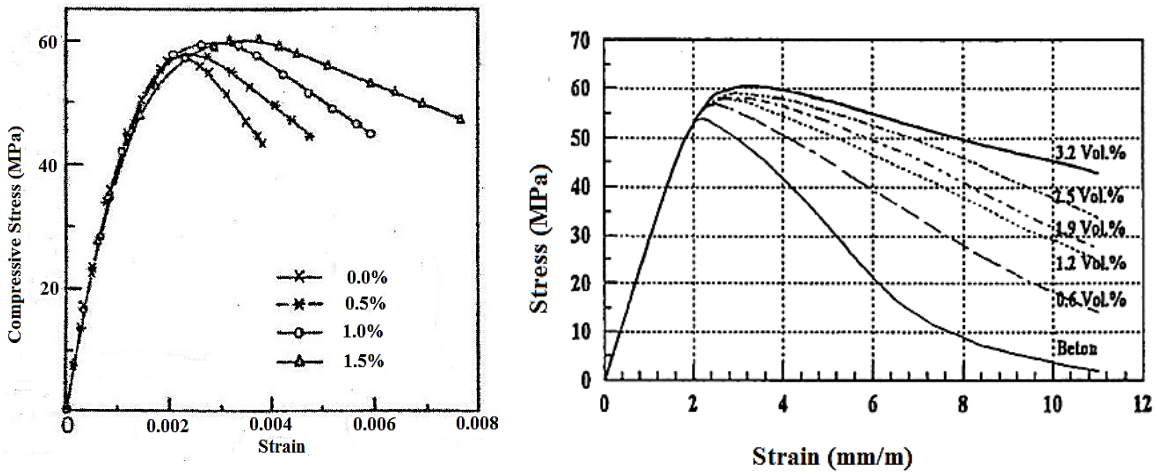

FIGURE 2–1. Effects of steel fibers content on compressive stress-strain curve of FRC ((Padmarajaiah & Ramaswamy, 2002) (left) and (Tejchman & Kozicki, 2010)

2.2 Steel Fiber Reinforced Concrete (SFRC)

The SFRC is a composite material made of cement, fine and coarse aggregates and discontinuous discrete steel fibers. It is a modified form of concrete wherein short and discrete steel fibers are dispersed in the concrete ingredients at the time of mixing (Singh, 2017) .

Steel fibers can be defined as discrete, short length of steel having ratio of its length to diameter (aspect ratio) in the range of 20 to 100 with any of the several cross-section, and that are sufficiently small to be easily and randomly dispersed in fresh concrete mix using conventional mixing procedure (Behbahani, et al., 2011).

The mechanical properties of steel fiber reinforced concrete are influenced by the type of fiber; length-to diameter ratio (aspect ratio); the amount of fiber; the strength of the matrix; the size, shape, and method of preparation of the specimen; and the size of the aggregate. For this reason, mixtures proposed for use in design should be tested, preferably in specimens representing the end use, to verify the property values assumed for design (ACI 544.4R, 1999).

The enhancement in the mechanical properties of the concrete because of the fiber mixing can be attributed mainly to their localized reinforcing capability, as their presence in the mortar matrix around coarse aggregates in the concrete arrests the opening, widening and later on, extension of the micro-cracks already existing therein to adjoining areas in the concrete mass (Singh, 2017). Figure 2.2 depicts a typical random distribution of the steel fibers in the concrete mix.

SRFC is being increasingly used in shotcrete as tunnel linings, precast structures, off-shore platforms, water retaining structures, structures in high seismic risk areas, bridges, industrial or factory pavements, highways, roads, parking areas, bridge decks, airports runways and also in versatile engineering structures. (Islam, et al., 2014)

The behavior of SFRC can be classified into three groups according to its application, fiber volume percentage and fiber effectiveness; for instance Behbahani, et al. (2011) classified

FIGURE 2–2. Steel fiber reinforced concrete section (Singh, 2017).

SFRC based on its fiber volume percentage as follows:

i. Very low volume fraction of Steel Fiber (less than 1% per volume of concrete), which has been used for many years to control plastic shrinkage and as pavement reinforcement.
ii. Moderate volume fraction of Steel Fibers (l% to 2% per volume of concrete) which can improve modulus of rupture, flexural toughness, impact resistance and other desirable mechanical properties of concrete.
iii. High volume fraction of Steel Fibers (more than 2% per volume of concrete) used for special applications such as impact and blast resistance structure.

According to Wafa (1990) classification Steel Fibers can be Straight, crimped, twisted, hooked, ringed, and paddled ends with diameter range from 0.25 to 0.76mm.

2.2.1 Compressive Behavior of SFRC

Similar to the normal concrete, the SFRC exhibits a linear-elastic behavior up to a stress level of 30 % of the ultimate concrete strength in compression. At this stage, the internal microstructure of the concrete remains more or less stable (Singh, 2017). The compressive strength of is more or less equal to the strength of plain concrete, but ductility increases significantly after cracking (Kooiman, 2000).

Singh (2017) studied that the effect of the steel fibers become significant and visible on the stress-strain response only after the stress level in the specimen is increased beyond the threshold level of a normal concrete i.e. 70 % of the ultimate concrete compressive strength. It is reported that SFRC is able to sustain a compressive strain value of 0.005–0.009 on failure and the corresponding failure stress improves to about $0.95\sigma_{cu}$ from a value of $0.85\sigma_{cu}$ taken for a normal concrete, where σ_{cu} is concrete cylinder strength (Singh, 2017).

2.2.2 Tensile Behavior of SFRC

The objective of fiber additions in concrete is often to obtain a ductile failure behavior and due to fiber addition, the tensile strength can be increased (Kooiman, 2000). Unlike a plain concrete, the SFRC exhibits a significant residual-tensile strength because of the contribution of the fibers embedded in the hardened concrete, although its first cracking strength is almost same as that of a plain concrete (Singh, 2017).

The SFRC member, however, during the loading process undergoes a considerable deformations and cracking before the failure. This all happens because of the fibers present uniformly in the concrete volume, almost in every possible direction that bridge the crack surfaces in the concrete member (Singh, 2017). The ultimate tensile strain and the compressive strain of SFRC range between 0.015–0.020 and 0.0035–0.0070, respectively (Singh, 2017).

2.2.3 Advantages of SFRC

The hardened product of SFRC unlike a plain concrete possesses improved mechanical properties with an enhanced post-cracking tensile resistance and the toughness because of the random distribution and orientation of the fibers in concrete caused at the time of mixing and its placement (Singh, 2017).

The advantages of Steel Fiber Reinforced Concrete (Mitu, n.d.).

- Enhancement of ductility and energy absorption capacity
- Improve internal tensile strength of the concrete due to bonding force.

- Increase the flexural strength, direct tensile strength and fatigue strength.
- Enhance shear and torsional strength
- Shock resistance as well as toughness of concrete

2.3 Moment Redistribution

Moment redistribution is an important concept in structural engineering, and is a measure of the ability of the section to maintain a constant moment whilst simultaneously rotating and redistributing moment to another region of the member (Haskett, et al., 2010).

Statically indeterminate structures fracture may occur only after the loss of geometric stability of the total system with formation of plastic hinges. A plastic hinge promotes development of deflections and increase of stresses in compressed area in the course of reinforcement flow. Following the formation of a plastic hinge, while the load is increasing, the bending moment redistribution between specific cross-sections will take place (Vasiliev, et al., 2017).

According to Park & Paulay (1974), it is possible to use a distribution of moments and forces different from that given by linear elastic structural analysis if the critical sections have sufficient ductility to allow redistribution of actions to occur as the ultimate load is approached.

Redistribution of moments is dependent on adequate ductility in plastic hinge regions. These plastic hinge regions develop at sections of maximum positive or negative moment and cause a shift in the elastic moment diagram. The usual result is a reduction in the values of maximum negative moments in the support regions and an increase in the values of positive moments between supports from those calculated by elastic analysis (ACI 318R-14, 2014).

The main advantage of redistribution is that the maximum positive moment can be increased and the maximum negative moment at supports can be reduced, thus the resulting in lesser congestion of steel at the supports (Varghese, 2005).

2.4 Moment – Curvature Response for RC

The moment–curvature relation of a section is uniquely defined according to the dimensions of the concrete section and the material properties of concrete and steel. Also, the gradient of the moment–curvature relation means the elastic bending stiffness *EI* which includes all the section properties in a typical loading condition (Kwak & Kim, 2002).

The typical moment–curvature relation for a lightly RC section (under-RC section) can be idealized to the trilinear relation as per Kwak & Kim (2002). The first stage is to cracking, the second to yield of the tension steel, and the third to the limit of useful strain in the concrete. The behavior of the section after cracking is dependent mainly on the steel content.

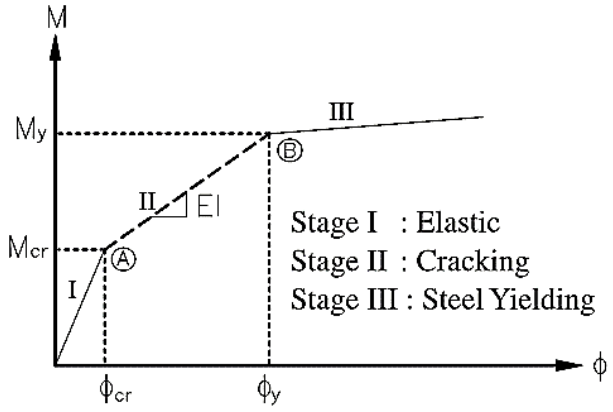

FIGURE 2–3. Idealized moment–curvature relation of RC section (Kwak & Kim, 2002).

From Varghese (2005) book it is stated that under simple bending theory the rotation of a section undergoes when a bending moment is applied. The rotation is then given by the following relation.

$$\frac{M}{I} = \frac{E}{R} = \frac{f}{y} \tag{2.1}$$

Taking x as the depth of neutral axis, we get

$$\frac{M}{EI} = \frac{1}{R} = \frac{\varepsilon_c}{E_c x} = \phi \tag{2.2}$$

Where strain in concrete is ε_c, $\varepsilon_c = f_c / E_c$

$$\phi = \frac{\text{Strain in extreme fiber}}{\text{Depth of neutral axis}} = \frac{\varepsilon_c}{x} \tag{2.3}$$

Similarly the moment- curvature diagram for reinforced concrete flexural members was developed by Park & Paulay (1974) as shown in Figure 2.4.

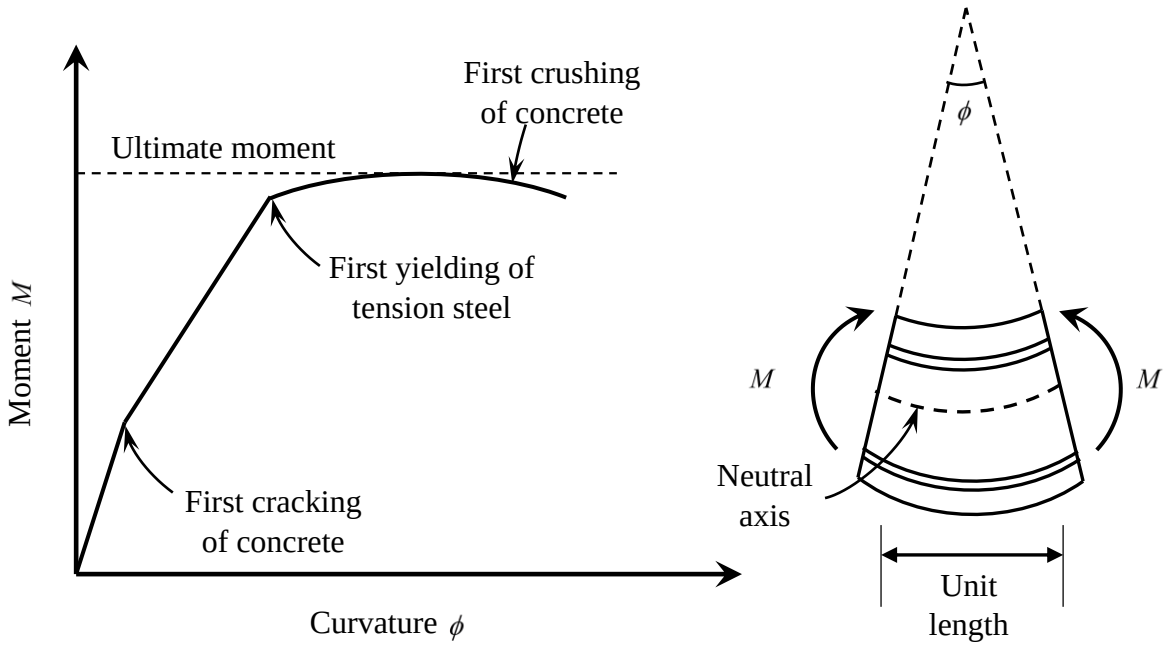

FIGURE 2–4. Typical Moment- curvature relationship for reinforced concrete flexural members (Park & Paulay, 1974).

2.5 Moment – Curvature Response for SFRC

The moment-curvature response of a beam is a measure of its toughness or energy absorption capacity. The curvature denotes a change of the slope that a member undergoes upon loading. It can be conveniently measured from the linear strain distribution in the member section as a ratio of the summation of the compressive strain in the extreme concrete fiber (ε_{cu}) and the strain prevailing at the centroid of the reinforcing rebars (ε_{st}) or extreme tensile face (ε_t) of an SFRC section to the member depth (*D*) (Singh, 2017). Moment-curvature response of a flexural member is formulated using material constitutive relationship describing the material response.

Singh (2017) studied and presented the following section analysis empirical expressions and formulas by using the stress-profile model, the most commonly adopted method to capture the flexural capacity of members. Figure 2-5 shows a schematic representation of an SFRC-beam section reinforced with the conventional longitudinal reinforcement on its tensile zone.

The starting point of the method is to assume a stress-profile for the member, both in tension and compression, depending upon the material characteristics. A linear-strain distribution is usually assumed along the depth of the flexural member. This condition is mostly met in practice for the flexural members having a span/ depth ratio of more than 2.5 (Singh, 2017).

The material constitutive model define the relationship between the strain values and the corresponding stresses mobilized at various points along the member depth. The stresses can be used to estimate the magnitude of the section forces (namely, compression and tensile) acting above and below the member neutral axis; the integration of the stress function used in the material constitutive model gives the resultant force and its point of application (Singh, 2017).

Singh (2017) section analysis of SFRC assumptions and formulations:

- A SFRC rectangular beam section having width (*B*) and depth (*D*) is considered.

- The quantity of the steel fibers in the beam section is expressed by means of a parameter, called as volume fraction (V_f), which defines the ratio of the volume of the steel fibers present in the section to the concrete volume.
- Steel fibers with an aspect ratio (l/d) are considered to be randomly distributed and presented uniformly in the entire section.
- Conventional longitudinal steel rebars having a cross-sectional area (A_{st}) are also considered to be present in the beam section at a distance (d') from its bottom face for a sake of completeness. By putting a zero value of tensile steel areas (A_{st}), the model can be used for the analysis of a SFRC beam section.
- Knowing the radius of curvature, r ($=\varepsilon/y$) of the beam, the strain (ε) at any level (y) from the neutral-axis of the beam can be determined. This is based on the fact that the plane section norm al to the beam- axis remains plane after bending for a member having a span/depth ratio of more than 2.5.

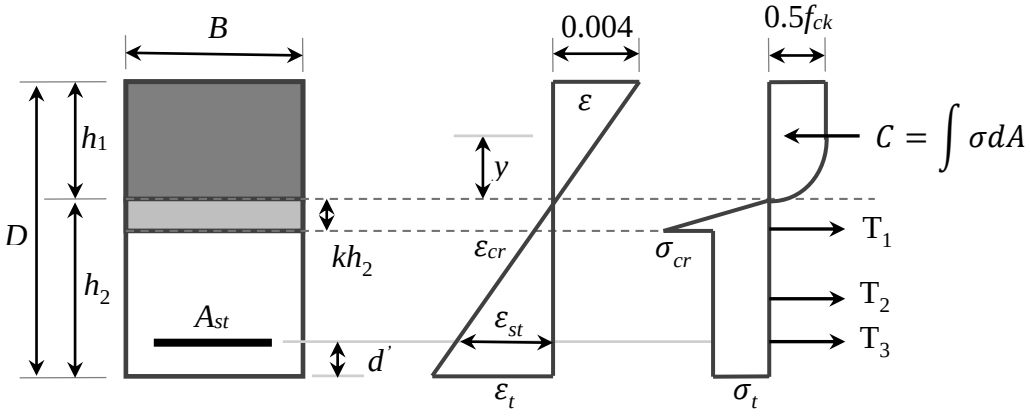

FIGURE 2–5. Stress-profile model of SFRC (Singh, 2017).

- The summation of h_1 and h_2, the position of the neutral-axis, denotes the depth (D) of the section
- The extreme strain values prevailing at the beam top face (ε_{cu}) and the beam bottom faces (ε_t) and/or strain at the level of the rebars (ε_{st}).

$$r = \frac{\varepsilon_{cu}}{h_1} = \frac{\varepsilon_t}{h_2} = \frac{\varepsilon_{st}}{d - h_1} = \frac{\varepsilon_{st}}{h_2 - d'} \tag{2.4}$$

From the above equation, the depth of the neutral axis (h_1) in the beam and the depth of the uncracked concrete zone (kh_2) existing in the beam section below its neutral axis can be determined.

The values of $(h_1/D)_b$ and $(h_2/D)_b$ define the position of the neutral axis in the balanced state, when the strain values at the top face of the beam (ε_{cu}) and at the level of the tensile steel (ε_{st}) in the beam reached, simultaneously. The position of the neutral axis in the balanced state of the SFRC beam can be determined using the similarity of the strain triangles existing above and below the neutral-axis of the beam section (Singh, 2017).

$$\left(\frac{h_1}{D}\right)_b = \left(\frac{\varepsilon_{cu}}{\varepsilon_{cu} + \varepsilon_{st}}\right)\frac{d}{D} \text{ and } \left(\frac{h_2}{D}\right)_b = \left(\frac{\varepsilon_{st}}{\varepsilon_{cu} + \varepsilon_{st}}\right)\frac{d}{D} \tag{2.5}$$

- The value of the constant k $(= \varepsilon_{cr}/\varepsilon_t)$.The value of the parameter (k) normally ranges from 0.0075 to 0.01. In practice, the value of the cracking-strain can be taken identical to that of a plain concrete (=0.00015). The value of the ultimate strain in tension should be adopted corresponding to the permitted crack-width at the ultimate limit state. It can be taken as 0.015 for SFRC in case the crack-width is not specified or SFRC experimental stress-CMOD response is unknown.

The principle of statics $\int_A \sigma \partial A = 0$ and $\int_A \sigma y \partial A = M$ can be used to calculate the actual position of the neutral-axis in the SFRC beam section and the corresponding moment capacity (M_u). The expanded version of these two expressions is given below (Singh, 2017):

$$\int_{h_2}^{h_1} \sigma \mathrm{B} \partial y = \mathrm{B}r \int_{h_2}^{h_1} \sigma \partial \varepsilon = 0 \tag{2.6}$$

The actual position of the neutral-axis of the beam can be determined by equating the areas of the compression zone (C) and the SFRC tension-stress block (a sum total of T_1 and T_2) along with the contribution from the conventional reinforcing rebars (T_3) present in the section (Singh, 2017).

$$C = T_1 + T_2 + T_3 \tag{2.7}$$

$$0.4167 f_{ck} h_1 B = \frac{1}{2}\sigma_{cr} k h_2 B + \sigma_t (1-k) h_2 B + \sigma_{st} A_{st} \tag{2.8}$$

$$\frac{h_1}{h_2} = \frac{0.5\sigma_{cr} k + \sigma_t (1-k) + \sigma_{st} p\left(\frac{D}{h_2}\right)}{0.4167 \xi f_{ck}}$$
$$h_1 + h_2 = D \tag{2.9}$$

A simplified form of equation 2.8 and 2.9 is given in Equation 2.10.

$$\xi \frac{h_1}{D} = \left(\frac{2.38\beta + 2.4\gamma\omega}{1 + 2.38\beta}\right) \text{ and } \frac{h_2}{D} = \left(1 - \frac{h_1}{D}\right) \tag{2.10}$$

$$\beta = \frac{\sigma_t}{f_{ck}} \text{ and } \omega = \left(\frac{A_{st}}{BD}\right)\frac{f_y}{f_{ck}} \tag{2.11}$$

Where $\beta =$ fiber-index, $\omega =$ reinforcement-index, $f_y =$ yield strength, f_{ck} = 28 days compressive strength, $\gamma =$ stress-mobilization factor for reinforcing rebars and $\xi =$ parameter that represents the effect of the steel fiber inclusion in the concrete on its crushing strain. $\xi = 1$ for SFRC and $\xi = 0$ for plain concrete.

The moment capacity (M_u) of the SFRC beam section can be determined using the equation of statics.

$$M_u = C\left(0.5833 h_1\right) + T_1\left(\frac{2}{3} k h_2\right) + T_2\left[h_2 - \frac{(1-k)h_2}{2}\right] + T_3\left(h_2 - d'\right) \tag{2.12}$$

Equation 2.12 can be simplified to a non-dimensional form as given in Equation 2.13 by substituting the values of C_1, T_1, T_2 and T_3.

$$\frac{M_u}{f_{ck}BD^2}=\left[0.24\xi\left(\frac{h_1}{D^2}\right)+\left(\frac{h_2}{D}\right)^2\left\{\alpha\beta+0.5\beta+\gamma\omega\left(\frac{D}{h_2}\right)\left(1-\frac{d'}{D}\frac{D}{h_2}\right)\right\}\right] \quad (2.13)$$

In Equation 2.14 α denotes a constant that considers the contribution of the uncracked concrete existing below the neutral-axis of the SFRC flexural member (Singh, 2017).

$$\alpha=\left[\frac{1}{3}\left(\frac{\sigma_{cr}}{\sigma_t}\right)k^2-\left(\frac{k}{2}\right)^2\right] \quad (2.14)$$

Generally, the value of (k) is too small to affect the overall analysis results. It is therefore always safer to ignore the contribution of the uncracked concrete existing below the neutral-axis. Accordingly, the value of the constant (α) can be ignored during the analysis without affecting the accuracy of the results. This process results in further simplification of Equation 2.13; it is given in Equation 2.15 (Singh, 2017).

$$\frac{M_u}{f_{ck}BD^2}=\left[0.24\xi\left(\frac{h_1}{D^2}\right)+\left(\frac{h_2}{D}\right)^2\left\{0.5\beta+\gamma\omega\left(\frac{D}{h_2}\right)\left(1-\frac{d'}{D}\frac{D}{h_2}\right)\right\}\right] \quad (2.15)$$

2.6 Moment – Rotation Relationship

The moment-rotation behavior describes the structural behavior of a flexural member in the process of hinge development. It provides an indication of the bending capacity and member ductility (Möhr, 2012).

According to Park and Paulay (1974) the rotation capacity at the center support is derived as follows. It is noted that all stage equilibrium requires that

$$M+\frac{M'}{2}=\frac{Pl}{4}\Leftrightarrow P=\frac{4}{l}\left(M+\frac{M'}{2}\right) \quad (2.16)$$

And, if the moment at the center support remains at M_u' until M_u develops at the mid-span sections, we have

$$P = \frac{4}{l}\left(M_u + \frac{M_u^{'}}{2} \right) \tag{2.17}$$

Therefore, if sufficient rotation capacity of the plastic hinges is available, the bending moment distribution at the ultimate load may be quite different from that calculated using elastic theory and depends on the ultimate moment resistance of the sections. In reinforced concrete structures, the ductility at the first plastic hinges formed may be insufficient to enable full redistribution of moments to take place with the ultimate moment at each critical section. Thus, if moment redistribution is to be relied on, the availability of sufficient ductility at the plastic hinges must be ensured (Park & Paulay, 1974).

As an example, from Park & Paulay (1974) book, the calculated required plastic rotation for the two-span continuous beam of Figure 2.6 for the case of the plastic hinge forming at the center support is considered. The beam and the curvature diagrams of Figures 2.6 (a) and 2.6 (b) indicate the stage at which sufficient plastic rotation has occurred at the center support, B, to enable the ultimate moment M_u to be just developed at mid-span. Hence Figures 2.6 (a) and 2.6 (b) indicate the stage when P_u is just reached. The plastic curvature is considered to occur over the equivalent plastic hinge length, l_p, each side of the critical section. The elastic curvature along the length of the member may be calculated from the distribution of bending moments and the assumed constant flexural rigidity, EI. The plastic rotation, θ_p at the centre support, *B*, is described as the discontinuity of the slope between the ends of the adjacent members, and $\theta_p = 2\theta_B$ as indicated in Figure 2.6 (a). θ_p is determined by considering the elastic deformations of the members supporting the loads P_u. First, the plastic hinge at *B* is replaced by a frictionless hinge as in Figure 2.6 (c). Then from the moment area theorem the rotation at *B* due to load P_u alone on one span is (Park & Paulay, 1974),

$$\theta^{'} = \frac{\left(M_u + 0.5M_u^{'} \right) l}{4EI} \tag{2.18}$$

The effect of the ultimate support moment, $M_u^{'}$, acting at the frictionless hinge, as in Figure 2.6 (d), can now be considered. The rotation at *B* due to $M_u^{'}$ alone is

$$\theta_B^{"} = \frac{M_u^{'} l}{3EI} \tag{2.19}$$

$$\theta_B = \theta_B^{'} - \theta_B^{"} = \frac{l}{4EI}\left(M_u - \tfrac{5}{6} M_u^{'}\right) \tag{2.20}$$

$$\theta_p = 2\theta_B = \frac{l}{2EI}\left(M_u - \tfrac{5}{6} M_u^{'}\right) \tag{2.21}$$

Equation 2.20 provides the rotation required at the plastic hinge at the center support *B* for the case when $M_u > \frac{5}{6} M_u^{'}$. If $M_u = \frac{5}{6} M_u^{'}$ the required θ_p is zero, because of this the ratio of moments is given by elastic theory, and no bending moment redistribution is required. Also, if $M_u < \frac{5}{6} M_u^{'}$ the value given for θ_p is negative, in that case, the foregoing calculation does not apply, because the first plastic hinge forms at the load points at mid-span and the required plastic rotation at those sections would have to be calculated (Park & Paulay, 1974). In the example, when $M_u > \frac{5}{6} M_u^{'}$, redistribution of the bending moments can take place until the ultimate moment develops at each critical section if

$$\frac{l}{2EI}\left(M_u - M_u^{'}\right) \leq 2\left(\frac{\varepsilon_c}{c} - \frac{\varepsilon_{ce}}{kd}\right) l_p \tag{2.22}$$

Where, $\varepsilon_c =$ the concrete strain at extreme compression fibre at the ultimate curvature, $\varepsilon_{ce} =$ the concrete strain at the extreme compression fibre when the yield curvature is reached, $c =$ is the neutral axis depth at the ultimate moment, $kd =$ the neutral axis depth when the yield curvature is reached and $l_p =$ the equivalent plastic hinge length, each side of the critical section (Park & Paulay, 1974).

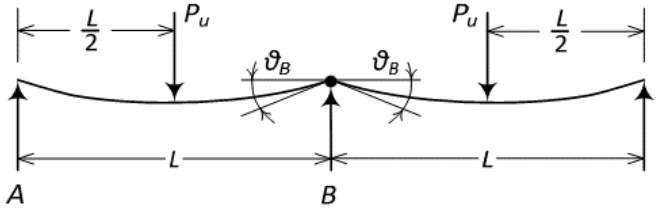

(*a*)

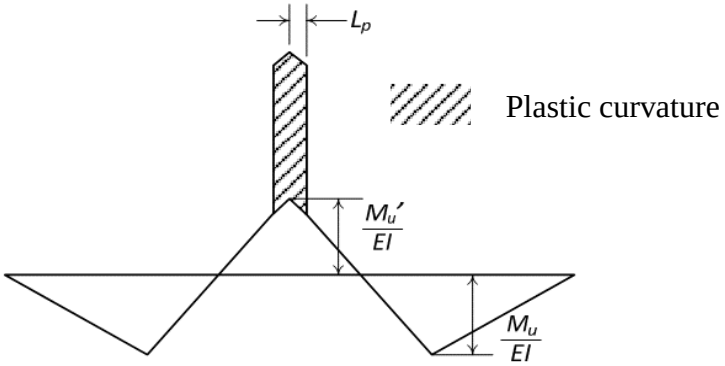

(*b*)

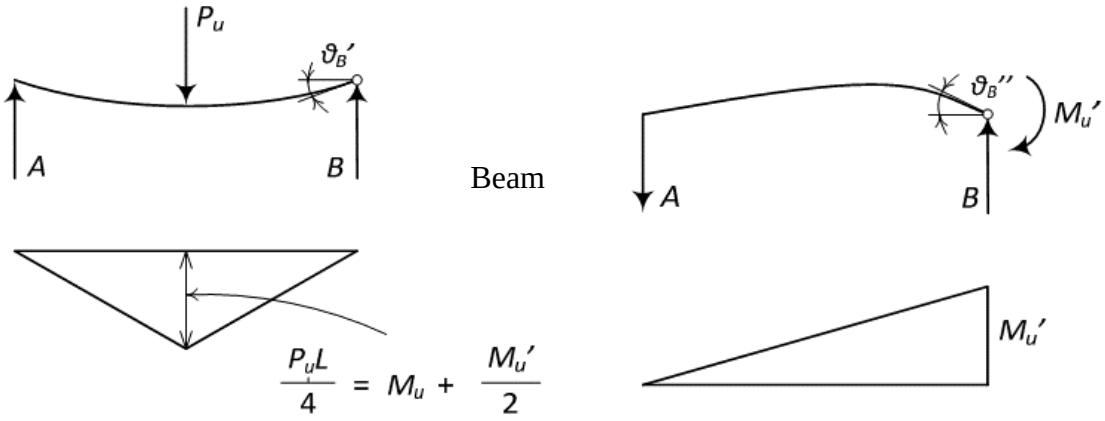

(*c*) Bending moments (*d*)

FIGURE 2–6. Plastic hinge rotation for continuous beam. (a) Deflected shape when ultimate load is reached. (b) Idealized curvature distribution when ultimate load is reached. (c) P_u acting without $M_u^{'}$. (d) $M_u^{'}$ acting without P_u (Park & Paulay, 1974).

Empirical expression for ultimate plastic rotation calculated from curvatures also proposed by Park and Paulay, (1974) from strain diagrams in Figure 2.7. The plastic hinge rotation to one side of critical section is

$$\theta_p = \left(\frac{\varepsilon_c}{c} - \frac{\varepsilon_{ce}}{kd} \right) l_p \tag{2.23}$$

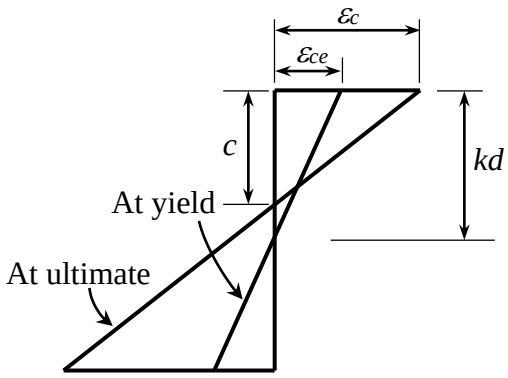

FIGURE 2–7. Strain diagrams at yield and ultimate curvatures (Park & Paulay, 1974).

2.7 Plastic hinge length and rotation

The method of calculation of idealized ultimate deformation/ rotation by Park and Paulay, (1974) in Figure 2-8 shows part of a reinforced concrete flexural member that has reached the ultimate curvature and bending moment at the critical section. End *A* of the member, for example, is the free end of a cantilever or a point of contra-flexure, and end *B* is a column face. The distribution of curvature along the member is apparent. The region of inelastic curvature is spread over a length of beam where the bending moment exceeds the yield moment of the section. The elastic contribution of curvature to the rotation over the full length of the member (the unshaded area of the curvature diagram of Figure 2.8 (c)) is given by

$$\theta = \int_A^B \frac{M}{EI} dx \tag{2.24}$$

$$\varphi = \frac{M}{EI} \tag{2.25}$$

where the flexural rigidity EI is given by an appropriate idealization. If a fully cracked section is assumed along the whole length of the member, EI is given by $E_c I_e = M_y / \varphi_y$, or approximately by M_u / φ_y.

$$I_e = \left(\frac{M_{cr}}{M_a}\right)^3 I_g + \left[1 - \left(\frac{M_{cr}}{M_a}\right)^3\right] I_{cr} \tag{2.26}$$

The shaded area of Figure 2.8(c) is the inelastic rotation that can occur at the "plastic hinge" in the vicinity of the critical section, thus representing the plastic rotation that occurs in addition to the elastic rotation at the ultimate stage of the member. The inelastic area at the ultimate stage can be replaced by an equivalent rectangle of height $\varphi_u - \varphi_y$ and width l_p, having the same area as the actual inelastic curvature distribution. The width l_p, is the equivalent length of the plastic hinge over which the plastic curvature is considered to be constant. φ_y and φ_u represent the yield curvature and the ultimate curvature, respectively.

The empirical expressions of equivalent plastic hinge length, l_p have been proposed by investigators as reviewed Park and Paulay, (1974).

(ES EN 2015) Figure 2.9 rotation capacity of beam zones undergo a plastic deformation (formation of yield hinges) under the relevant combination of actions over a length of approximately 1.2 times the depth of section.

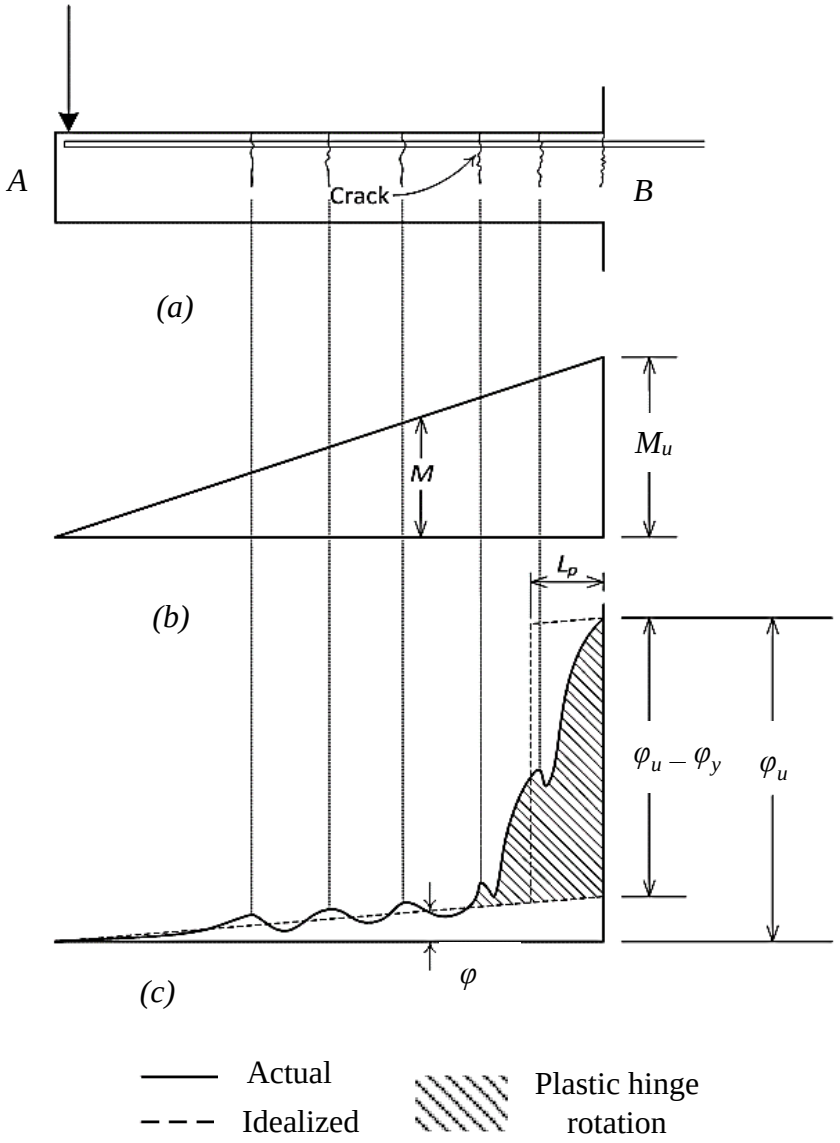

FIGURE 2–8. Curvature distribution along beam at ultimate moment. (a) Beam. (b) Bending moment diagram. (c) Curvature diagram (Park & Paulay, 1974).

For members with unconfined concrete Baker A. L., (1956) proposed the equation for equivalent plastic hinge length as

$$l_p = k_1 k_2 k_3 \left(\frac{z}{d}\right)^{0.25} d \tag{2.27}$$

where $k_1 = 0.7$, $k_2 = 1$, $k_3 = 0.6$ when $f_c^{'} = 35.2\,\text{MPa}$ or 0.9 when $f_c^{'} = 11.7$ MPa,

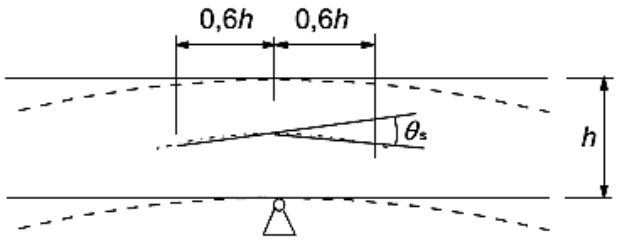

FIGURE 2–9. Plastic rotation of reinforced concrete sections for continuous beams (ES EN, 2015)

assuming $f_c^{'} = 0.85 \times$ cube strength of concrete.

From the results of tests on simply supported beams, Corley W. G., (1966) has proposed the following expression for the equivalent length of plastic hinge:

$$l_p = 0.5d + 0.2\sqrt{d}\left(\frac{z}{d}\right) \tag{2.28}$$

Where $z =$ distance from critical section to the point of contraflexure, $d =$ effective depth of beam in (inches).

In discussing Corley's paper, Mattock A.H., (1967) suggested that the simple form of equivalent plastic hinge length is

$$l_p = 0.5d + 0.05z \tag{2.29}$$

Sawyer H.A., (1964) has proposed the following expression for the equivalent length of plastic hinge:

$$l_p = 0.25d + 0.075z \tag{2.30}$$

This equation is based on the assumptions that the maximum moment in the member is the ultimate, that $M_y / M_u = 0.85$, the zone of yielding is spread $d/4$ past the section in which the bending moment is reduced to M_y.

2.8 Moment Redistribution Calculation

Theoretically moment redistribution occurs when the structure's response deviate from that of an elastic response, which implies that moment redistribution initiates after cracking occurred. The amount of moment redistribution is seen to be proportional to the difference between the failure bending moment (M_u) and the elastic bending moment (M_e) (Möhr, 2012).

Moment redistribution involves adjustment of the bending moment distribution obtained from a linear elastic analysis with the difference between the redistributed and initial bending moment diagrams being an indicator of the amount of redistribution which has occurred (Scott & Whittle, 2005). The percentage of moment redistribution at a section along a beam is calculated as follows:-

$$\%\text{Redistribution} = \left(\frac{\text{Moment after Redistribution} - \text{Moment before Redistribution}}{\text{Moment before Redistribution}} \right) \times 100 \qquad (2.31)$$

For illustration, a two-span continuous beam, having a uniform cross section as shown in Figure 2.10, is considered (Park & Paulay, 1974). $M_u^{'}$ is the ultimate moment of resistance of the negative bending moment sections (hogging sections) and M_u the ultimate moment of resistance of the positive bending moment sections (sagging sections). It is assumed that the moment-curvature relationship for the sections is the idealized bilinear relationship for a ductile section shown in Figure 2.10 (b), with all sections having the same constant flexural rigidity up to the ultimate moment and the moment remaining constant at the ultimate value at higher curvatures. At relative low loads the distribution of bending moment due to the two concentrated loads is in accordance with the elastic theory distribution as shown in Figure 2.10 (c). The self-weight of the beam is neglected in the calculation of the moment distribution. As the applied loads are increased further, the ultimate moment of resistance is reached at a critical section, for this scenario it would be over the center support, before it is reached at the other sections. Then the moment at the center support is $M_u^{'}$, as in Figure 2.10 (d). The extent to which further load can be carried

by the beam depends on the capacity for plastic rotation at the center support. If the section is brittle, the moment will decrease rapidly after reaching the maximum capacity (as in Figure 2.10 (d)), and the beam will fail suddenly without carrying any additional load. If the section is ductile, additional load can be carried because the plastic hinge at the center support rotates while maintaining its moment of resistance constant at $M_u^{'}$, and moment redistribution will occur until the maximum positive moment in the spans increases to M_u. At this instant the collapse mechanism in Figure 2.10 (e) is formed. Figure 2.10 (f) traces the variation of bending moment at the critical sections with load on the beam, assuming that the plastic hinge develops at the center support (this requires $M_u^{'}/M_u \leq M^{'}/M = 1.2$) (Park & Paulay, 1974).

2.9 Permissible Moment Redistribution

The design values implemented for the allowable amount of moment redistribution differ among various design codes. Design codes allow the moment redistribution to be measured relative to the designed neutral axis depth (Möhr, 2012). Figure 2.11 provides an overview of the current design values for moment redistribution as applied in different codes.

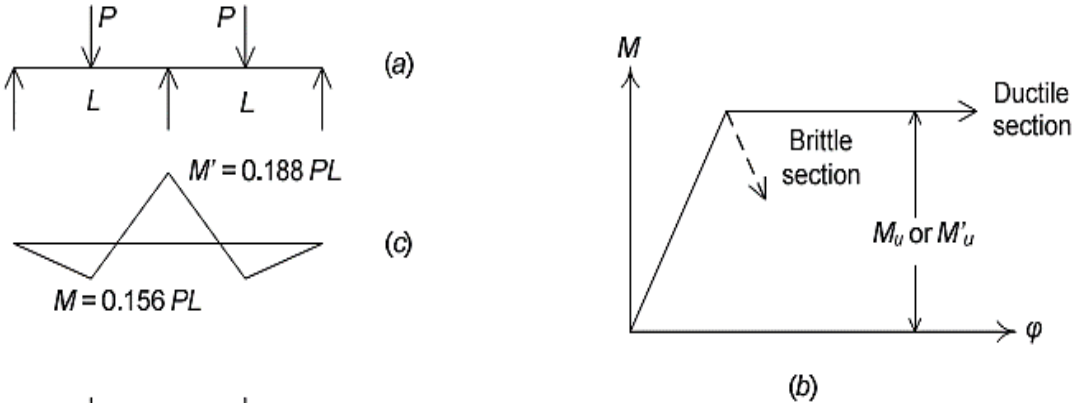

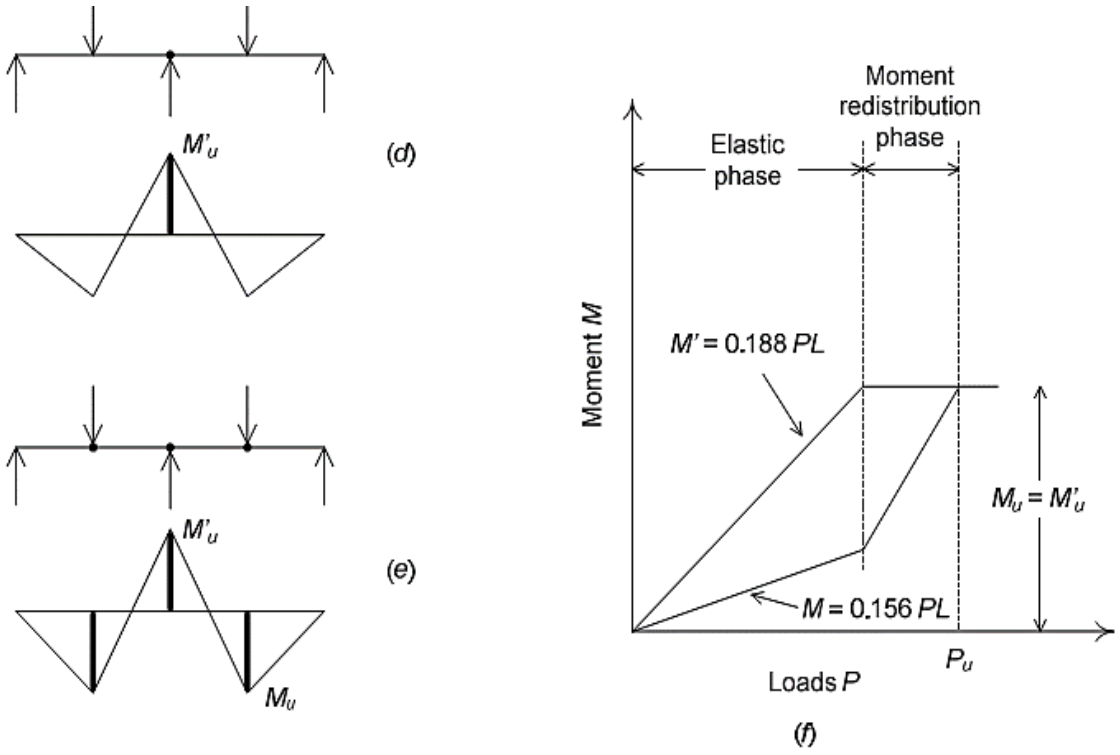

FIGURE 2–10. Moment Redistribution and formation of collapse mechanism for a continuous beam. (a) Beam. (b) Idealized Moment-curvature relationship for sections. (c) Elastic theory bending moment diagram. (d) At formation of first plastic hinge. (e) At formation of collapse mechanism. (f) Change of bending moment with load (Park & Paulay, 1974).

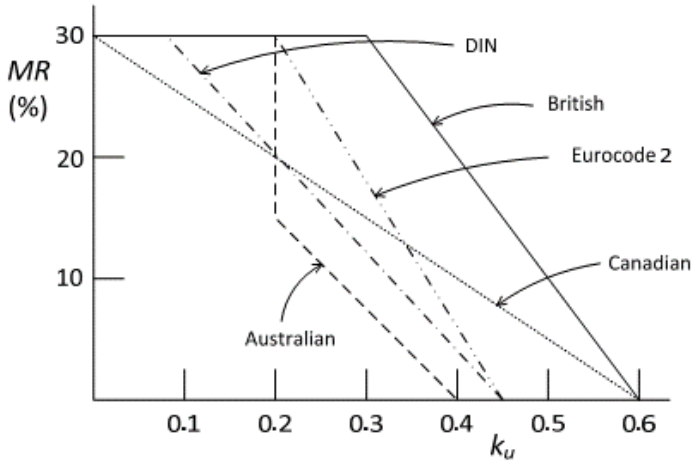

FIGURE 2–11. Prescribed moment redistribution according to neutral axis depth approach (Möhr, 2012)

According to the ES EN, (2015) moments at the ultimate limit state (ULS) calculated using linear elastic analysis may be redistributed, provided that the resulting distribution of moments remains in equilibrium with the applied loads. In continuous beams which are predominantly subjected to flexure and have the ratio of lengths of adjacent spans in the range of 0.5 to 2, redistribution of bending moments without an explicit check on the rotation capacity, provided that:

$$\delta \geq k_1 + k_2 \frac{x_u}{d} \qquad \text{for} \quad f_{ck} \leq 50 \text{ MPa} \tag{2.32}$$

$$\delta \geq k_3 + k_4 \frac{x_u}{d} \qquad \text{for} \quad f_{ck} > 50 \text{ MPa} \tag{2.33}$$

$\delta \geq k_5$ where Class B, Class C or Class D reinforcement is used (see Annex C) and $\delta \geq k_6$ where Class A reinforcement is used see Annex C (ES EN 2015). Where $\delta =$ the ratio of the redistributed moment to the elastic bending moment, $x_u =$ the depth of the neutral axis at the ULS after redistribution, $d =$ the effective depth of the section, $k_u =$ neutral axis depth.

The recommended value for $k_1 = 0.44$, $k_2 = 1.25(0.6 + 0.0014/\varepsilon_{cu2})$, $k_3 = 0.54$, $k_4 = 1.25(0.6 + 0.0014/\varepsilon_{cu2})$, $k_5 = 0.7$ and $k_6 = 0.8$. Where $\varepsilon\varepsilon_{cu2} =$ ultimate strain.

2.10 Modelling of SFRC member using FEA

To design complicated SFRC structural elements, it is necessary to employ non-linear FEA. The concrete constitutive model and the representation of the cracks are the main parameters affecting the accuracy of FEA of concrete (Tlemat, et al., 2006). The structural response of SFRC elements is characterized by its tensile strain-softening behavior. A number of available constitutive models for SFRC have been identified such as those proposed by RILEM, Barros, Lok, Tlemat and others (Abbas, et al., n.d.)

According Tlemat, et al (2006) and researchers commercially available FEA packages (e.g. DIANA, ATENA, ANSYS and ABAQUS) use the stress-displacement or stress-strain

relationship to describe the tension softening of the concrete in the cracked region. The cracking process can be represented by two approaches.

The first approach uses the discrete crack representation model, which is based on the stress-displacement concept. This method is more precise as far as local post-crack behavior is concerned, but it is computationally more intensive and less useful when trying to develop design models for practical applications (Tlemat, et al., 2006).

The second approach is smeared crack approach which assumes cracks to be smeared out over the element ($\sigma - \varepsilon$ method). The main disadvantage of this model is that, in particular for small amounts of flexural reinforcement, it introduces mesh sensitivity in the analysis, since mesh refinement will lead to narrower crack bands. To obtain the ideal stress-strain characteristics of concrete, an ideal uniaxial tensile test should be performed. Results from flexural tests can be used to develop the stress-strain or stress-crack width characteristics for FEA modelling (Tlemat, et al., 2006).

CHAPTER THREE

RESEARCH METHODOLOGY

The study used two methods. The first method was experimental program that aimed at obtaining material properties and characteristics of SRFC with volume addition of 0%, 0.5%, 0.75% and 1.5% steel fibers, compressive strength behavior and tensile strength behavior, which used as input data for modelling of continuous beam. It provided SFRC material constitutive models (moment-curvature response and moment-rotation response). The second method was modelling the beam using finite element modelling analysis, FEA in Abaqus CAE software. To provide an indication of the amount of moment redistribution it was required to create a finite element model of a statically indeterminate structure that implements the derived moment-curvature response.

3.1 Strength and Mechanical Properties of Hardened Concrete

3.1.1 Test Program for the Compressive Strength Behavior of SFRC

In this study, the compression test with standard cubes specimens with dimensions (150 × 150 ×150) mm for length, width, height respectively was conducted to investigate the compressive behavior of SFRC. The variables were concrete compressive strength, fiber volumetric ratio, and fiber aspect ratio. Four fiber volumetric ratios 0%, 0.5%, 0.75% and 1.5% were considered, and waste steel fibers with aspect ratios of (50-60) were used. The addition of steel fibers was done per volume of total mix proportion. In order to investigate the effect of concrete compressive strength, compressive strength of 25 MPa was targeted.

The compressive strength test was carried out in Construction Material Laboratory of Jimma institute of Technology for both fibrous and non-fibrous (control) concrete. The specimens were loaded uni-axially using the Universal Compression Testing machine.

Three cube specimens per test series were casted, which resulted in 12 specimens for 4 test series. The specimens were demolded one day after casting and then cured until the age of 28 days, when the compression tests were conducted. To prevent the specimens from being

subjected to possible eccentric loading, both the top and bottom surfaces of all specimens were ground. The specimens were subjected to uniaxial compression .

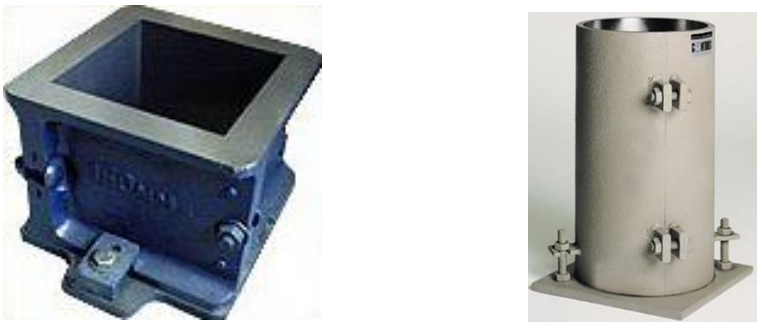

FIGURE 3–1. Cube mold (Left) and Cylinder mold (Right).

3.1.2 Test Program for the Splitting Tensile Strength Behavior of SFRC

The tensile response of a material was evaluated using indirect tensile test method, splitting tensile strength test. Indirect tensile strength (Splitting tensile strength) was carried out in Construction Material Laboratory of Jimma institute of Technology on non-fibrous (control), and fibrous concrete specimens using standard cylinders specimens with (100) mm diameter and (200) mm height. The test carried out by placing a cylinder specimen horizontally in the compression testing machine and load applied until failure occurred. The splitting tensile strength was calculated from the following equation:

$$\sigma_t = \frac{2P}{\pi LD} \tag{3.1}$$

Where:

$\sigma_t =$ Splitting tensile strength (MPa), $P =$ applied compressive load (N), $L =$ Length of cylinder (mm) and $D =$ Diameter of cylinder (mm).

Three cylinders specimen per test series were casted, which resulted in 12 specimens for 4 test series. The specimens were demolded one day after casting and then cured until the age of 28 days, when the splitting tensile strength tests were conducted.

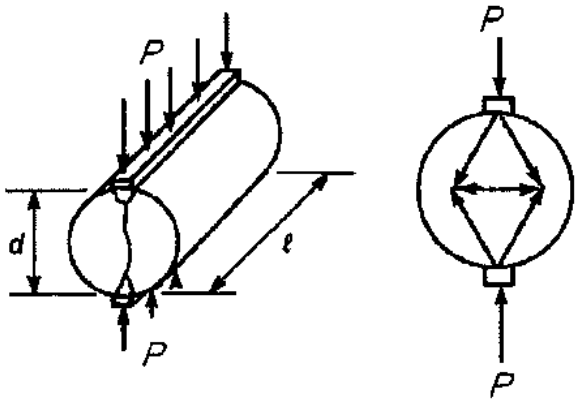

FIGURE 3–2. Sample split cylinder specimen and applied load.

3.2 Concrete Mix Design and Proportioning

Concrete mix design was done to find the right proportions of cement, sand and aggregates for concrete to achieve target strength in structures.

The aim of designing the mix was to determine the most economical and practical combination of readily available materials to produce a concrete that satisfied the performance requirements under particular conditions of use. The concrete mix design involved various steps, calculations and laboratory testing to find right mix proportions.

Proportioning of a concrete mix consisted of determining the relative amounts of materials which produced a concrete of desired workability of the fresh concrete, and the desired strength, consistency of volume, durability, and economy in the hardened concrete.

3.2.1 Material characteristics and properties

Characterizing properties of materials were based on their physical and chemical composition. The physical properties have done in laboratory for fine and coarse aggregate materials used in mix proportion and for cement the properties have taken from factory catalogue. The properties of steel fiber material used in the study was also discussed under this section.

3.2.1.1 Cement

As mixture cement was a binder, hardens, and adheres to other materials to bind them together. Cement powder reacted with water and its composition gradually changes and the particles of cement bind together and adhere strongly to materials with which they are mixed. Cement hardens gradually after it was mixed with water. In this study Ordinary Portland Cement (OPC) manufactured by Dangote Cement PLC. was used.

3.2.1.2 Fine Aggregate

Fine aggregate used in the study was natural sand which has been sieved to remove particles larger than 4.75 mm. The purpose of the fine aggregate was to fill the voids in the coarse aggregate and to act as a workability agent. The physical properties of fine aggregate: Silt content, moisture content, specific gravity and fineness modulus (sieve analysis) have done and the summary of experimental results are tabulated in table below. The other experimental results were attached in appendix.

3.2.1.3 Course Aggregate

In concrete, an aggregate was used for its economy factor, to reduce any cracks and most importantly to provide strength to the structure. It also Increases the volume of concrete, thus reduces the cost, provide dimensional stability Influence hardness, abrasion resistance, elastic modulus and other properties of concrete to make it more durable, strong and cheaper.

In conducting the study strong, dense, clean and free from any vegetable type coarse aggregate having average size of 20 mm were used. The aggregates were washed to keep the quality. Specific gravity, fineness modulus, water absorption and unit weight laboratory tests were performed.

TABLE 3–1. Fine Aggregate Properties

S.No.	Description	Test Result	Recommended Value
1	Type of Fine Aggregate	Natural Sand	Good Quality
2	Silt Content (%)		≤ 6%
3	Moisture Content (%)	1.13	Reducing water in mix
4	Specific Gravity	2.63	-
5	Absorption (%)	2.46	2.5-3.5
6	Unit weight (kg/m^3)	1528.5	
7	Fineness Modulus (%)	2.83	< 3

Their results summary are tabulated in table below and other experimental results were attached in appendix.

TABLE 3–2. Coarse Aggregate Properties

S.No.	Description	Test Result
1	Type of Coarse Aggregate	Manufactured aggregate
2	Moisture Content (%)	1.0
3	Specific Gravity (%)	2.91
4	Water Absorption (%)	1.01
5	Unit weight(kg / m^3)	1670.0

3.2.1.4 Water

In conducting the study municipal water was used in mixing and curing of concrete. Mixing water was the quantity of water that comes in contact with cement, impacts slump of concrete and was determined from water to cement ratio as per ACI mix design Specification.

3.2.1.5 Steel Fiber

Steel fibers wastage or byproduct from metallurgy were used. The steel fibers waste were collected from the mill and directly brought to laboratory, the effect of corrosion after mixing was not considered but steel fibers used were not corroded by exposure during storage. There were two shapes, straight and coil spiral, of waste steel fibers selected for mix purpose. Based on ACI (544) specification of steel fibers, aspect ratio (l/d) was fixed to 50 - 60. For straight steel fibers the thickness was used as *d* and for coil spiral steel fiber coil diameter was used as *d* in calculating aspect ratio. The waste steel fibers inherit the material properties of the main structural steel, basically elastic-perfectly plastic model was adopted due to its adequate accuracy and simplicity. Poisson's ratio was set to 0.3. A realistic density of 7850 kg/m^3 is adopted. Young's modulus was assigned as 205000 MPa.

Coarse aggregate

Fine aggregate/sand

Waste Steel Fiber

Fresh SFRC Concrete

FIGURE 3–3. Mix materials and fresh SFRC concrete.

3.3 Compressive stress – strain responses of SFRC

The compressive stress-strain response for SFRC was obtained from load-displacement response that measured from compressive strength test.

For the calculation of strain equation proposed by Singh H., (2017) was used because it is important to note the SFRC flexural members generally exhibit a linear relationship between the strain (ε) and the maximum deflection (δ). The following equation was used to derive the strain value from the deflection values observed during the tests.

$$\delta = 72.04\varepsilon + 0.02 \tag{3.2}$$

Modulus of elasticity, E for SFRC was calculated using equation confirmed by Collins, et al., (1993.

$$E = 3320\sqrt{f_{ck}} + 6900 \text{ for } f_{ck} \leq 100 \text{ MPa} \tag{3.3}$$

where f_{ck} = compressive strength of concrete.

3.4 Moment – Curvature Response Determination

The objective of response determination for moment-curvature of a beam was to measure its moment resistance capacity and curvature.

3.4.1 General Material Properties and Dimensions

TABLE 3–3. Material properties and dimensions for $M-\varphi$ response

Beam parameters	SFRC Beam			
	0 %	0.5 %	0.75 %	1.5 %
Size of SFRC beam ($B \times D$) (mm)	150×250	150×250	150×250	150×250
Span of the beam (mm)	1450	1450	1450	1450
Fiber volume fraction, V_f (%)	0	0.5	0.75	1.5
Fiber aspect ratio, l/d	50	50	50	50
Conventional tensile rebars detail	$2\phi 16$ mm	$2\phi 16$ mm	$2\phi 16$ mm	$2\phi 16$ mm
Cracking strain value, ε_{cr}	0.0001	0.0001	0.0001	0.0001

Concrete modulus of elasticity, E (MPa)	24370	26570	26870	23920
Cracking tensile strength of the concrete, $\sigma_{cr} = \varepsilon_{cr} E$ (MPa)	2.44	2.66	2.69	2.39
Concrete compressive strength, f_{ck}	27.69	35.10	36.18	26.92
Yield strength of tensile rebars, f_y (MPa)	415	415	415	415
Depth ratio $= \frac{d'}{D}$	0.1	0.1	0.1	0.1

3.4.2 Empirical expressions and formulas used

The following expressions and formulas were, which taken from Singh (2017), used for analysis.

i. Neutral axis positions calculation at balanced state

$$\left(\frac{h_1}{D}\right)_b = \left(\frac{\varepsilon_{cu}}{\varepsilon_{cu} + \varepsilon_{st}}\right)\frac{d}{D} \text{ and } \left(\frac{h_2}{D}\right)_b = \left(\frac{\varepsilon_{st}}{\varepsilon_{cu} + \varepsilon_{st}}\right)\frac{d}{D} \tag{3.4}$$

ii. Neutral axis positions calculation

$$\xi\frac{h_1}{D} = \left(\frac{2.38\beta + 2.4\gamma\omega}{1 + 2.38\beta}\right) \text{ and } \frac{h_2}{D} = \left(1 - \frac{h_1}{D}\right) \tag{3.5}$$

iii. Curvature calculation

$$\varphi = \frac{\varepsilon_{cu}}{h_1} = \frac{\varepsilon_t}{h_2} = \frac{\varepsilon_{st}}{d - h_1} = \frac{\varepsilon_{st}}{h_2 - d'} \tag{3.6}$$

iv. Moment capacity calculation

$$M_u = C\left(0.5833h_1\right) + T_1\left(\frac{2}{3}kh_2\right) + T_2\left[h_2 - \frac{(1-k)h_2}{2}\right] + T_3\left(h_2 - d'\right) \tag{3.7}$$

v. Non – dimensional moment capacity calculation

$$\frac{M_u}{f_{ck}BD^2} = \left[0.24\xi\left(\frac{h_1}{D^2}\right) + \left(\frac{h_2}{D}\right)^2 \left\{ \alpha\beta + 0.5\beta + \gamma\omega\left(\frac{D}{h_2}\right)\left(1 - \frac{d'}{D}\frac{D}{h_2}\right)\right\}\right] \quad (3.8)$$

3.5 Moment – Rotation Response Determination

The objective was to obtain the moment-rotation response that describes the structural behavior of a flexural member in the process of hinge development. It provided an indication of the bending capacity and member ductility.

Based on the mechanical properties of materials, plastic rotation capacity, θ_p at the center support of the beam was calculated as the integral of curvatures after reinforcement yielding along the hinge as follows from concept provided by Park & Paulay (1974).

$$\theta_p = \int_{l_p} \varphi dx \quad (3.9)$$

$$\theta_p = \left(\varphi_u - \varphi_y\right) l_p \quad (3.10)$$

$$\varphi_y = \frac{f_y}{E_s(1-k_y)d}, \quad \varphi_u = \frac{\varepsilon_{cu}}{h_1} \quad (3.11)$$

$$k_y = \sqrt{\left(n^2A^2 + 2nB\right)} - nA, \quad A = \rho + \rho', \quad B = \rho + \rho'\delta', \quad N = \frac{E_s}{E_c}, \quad \delta' = \frac{d'}{d} \quad (3.12)$$

Where φ_y and φ_u are the curvatures at the critical section at yield and ultimate respectively, l_p is the effective hinge length, k_y is the compression zone depth at yield normalized to *d*, ρ and ρ' are the reinforcement ratios of the tension and compression (normalized to *bd*) respectively, ε_{cu} is the ultimate concrete strain at extreme compression fiber, *d* is the effective depth of a cross section and h_1 is the depth of the neutral axis.

Equivalent plastic hinge length, l_p to one side of the critical section was obtained according to Mattock A.H., (1967),

$$l_p = 0.5d + 0.05z \tag{3.13}$$

3.6 Modelling of Moment Redistribution, Abaqus/CAE Software

This section described the development of a finite element model of the statically indeterminate member. A two-span continuous beam was modelled using the finite element analysis software, Abaqus/CAE 6.13. The aim was to predict the amount of moment redistribution experienced.

3.6.1 Failure Mechanism

For a statically indeterminate beam to collapse, more than one plastic hinge should be developed, so the study assumed three plastic hinges were developed for continuous beam to fail.

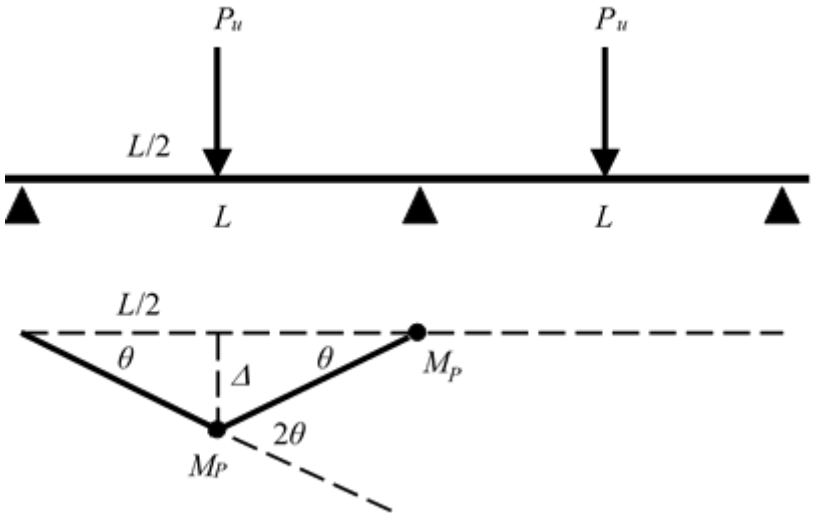

FIGURE 3–4. Failure mechanism of continuous beam

The plastic hinge acted as real hinge for further increase of load (until sufficient plastic hinges were developed for collapse). As the load increased, there was a redistribution of moment, as the plastic hinge cannot carry any additional moment.

Plastic hinges developed at the center support first, then the span beam becomes a simple beam, finally after plastic hinge developed at the center of the spans the beam collapsed.

The ultimate/collapse load, P_u was computed from Virtual-work method from collapse mechanism of the beam.

$$P_u = \frac{6M_p}{L} \tag{3.14}$$

$$M_P = \sigma_y \left(\frac{BD^2}{4} \right) \tag{3.15}$$

where P_u = collapse load, M_p = Plastic moment, σ_y = yield stress, and B = width and D = depth of the cross-section

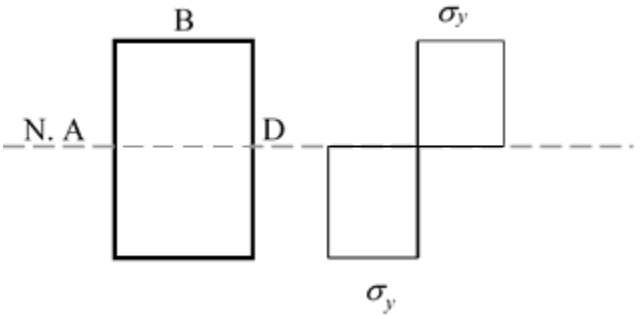

FIGURE 3–5. Stress distribution in a symmetrical cross section at fully plastic stage

3.6.2 Geometry

The layout of the modelled structure is shown in Figure 3.6. The beams dimensions were chosen to be : Span length (L): 1450 mm, beam width (*B*): 150 mm, beam height (*D*): 250 mm the total length of the beam is 3100 mm with a span length to height (L/h) ratio of 5.8. The section height to width (h/b) ratio is equal to 1.67. Over-hang (a): 100 mm.

3.6.3 Elements and Meshing

For modelling of continuous beam three-dimensional deformable part that can deform under mechanical concentrated load was used. The mesh module provides a variety of tools that allowed to specify different mesh characteristics, such as mesh density, element shape, and element type.

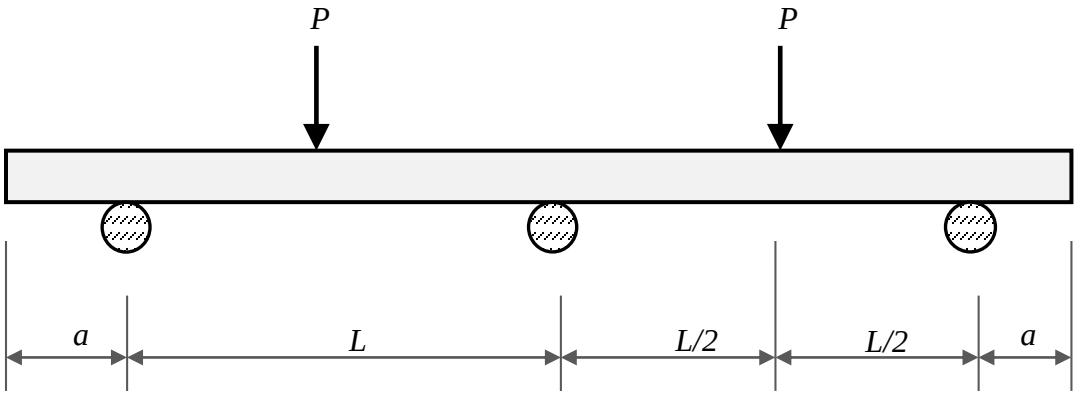

FIGURE 3–6. Layout of Modelled Beam.

3.6.4 Boundary Conditions

The boundary conditions were defined to induce symmetrical structural behavior. The displacement at the node representing the center support is constrained in the x- and y-direction to ensure the stability of the structure. The side supports were only constrained in the y-direction to allow for the horizontal movement of the member. These nodes were also defined to rotate freely. The nodes at the mid-spans were used to define the prescribed displacements.

3.6.5 Material Properties

For the analysis of five point bending test, the material property provided for the beam elements were the representative moment-curvature relationships. It was assumed that yielding occurs first at the center support by means of collapse mechanism which induces a plastic hinge formation.

3.6.6 Analysis Procedure

A displacement controlled procedure was performed. The nodes at the mid-spans were prescribed with a vertical displacement of 20 mm. The first crack was expected at the center support. The necessary results were the bending moment distribution, the reaction forces and the corresponding displacements. The results were checked for load controlled procedures after the peak load calculated was applied.

TABLE 3–4. Input data and parameters for FEA,Abaqus/CAE

Input	Volume of steel fiber			
	0 %	0.5 %	0.75 %	1.5 %
Size of SFRC beam ($B \times D$) (mm^2)	150×250	150×250	150×250	150×250
Span of the beam (mm)	1450	1450	1450	1450
Number of span	2	2	2	2
Modelling space	3D	3D	3D	3D
Concrete modulus of elasticity, E (MPa)	24370	26570	26870	23920
Mass density (10^{-6} kg/mm^3)	2.472	2.438	2.517	2.433
Concrete compressive strength, f_{ck}	27.69	35.10	36.18	26.92
Mesh type	C3D8	C3D8	C3D8	C3D8

Appendix B should be referred for detail Abaqus/CAE input data and other relevant information.

Abaqus/ CAE 6.13 Concrete Damage Plasticity was used to model the continuous SFRC beam. The following default parameters of Concrete Damage Plasticity model used were taken from Kmiecik & Kaminski (2011).

- Dilation angle $= 36^{\circ}$: Parameter characterizing the performance of concrete under compound stress
- Eccentricity $= 0.1$: The ratio of tensile strength to compressive strength
- $f_{bo} / f_{co} = 1.16$: The ratio of the compression strength in the biaxial state to the strength in the uniaxial state
- $\kappa = 0.667$
- Viscous parameter $= 0$

Compressive stress data were provided as a tabular function of inelastic (or crushing) strain, $\tilde{\varepsilon}_{in}^{c}$,

$$\tilde{\varepsilon}_c^{in} = \varepsilon_c - \varepsilon_{0c}^{el}$$
$$\varepsilon_{0c}^{el} = \frac{\sigma_c}{E_0} \tag{3.16}$$

where $\tilde{\varepsilon}_{in}^{c}$ = inelastic strain, ε_c = total strain ε_{0c}^{el} = elastic strain corresponding to the undamaged material (Abaqus/CAE, 6.13).

3.6.7 Calculation of Moment Redistribution

The amount of moment redistribution was seen to be proportional to the difference between the failure bending moment, M_u and the elastic bending moment, M_e.

The amount of moment redistribution was calculated using the same equations used by Möhr (2012), Oehlers (2006) and Liu, et al., (2006).

$$MR = (1-\delta)\times 100 \tag{3.17}$$

$$\delta = \frac{M_{red.}}{M_e} \tag{3.18}$$

where $M_{red.}$ = the value of the redistributed bending moment at the center support, M_e = the value of the elastic bending moment at the center support and δ = the ratio of redistributed bending moment to elastic bending moment.

The elastic bending moment, M_e was calculated using the formula given in figure below taken Park and Pauly (1974)

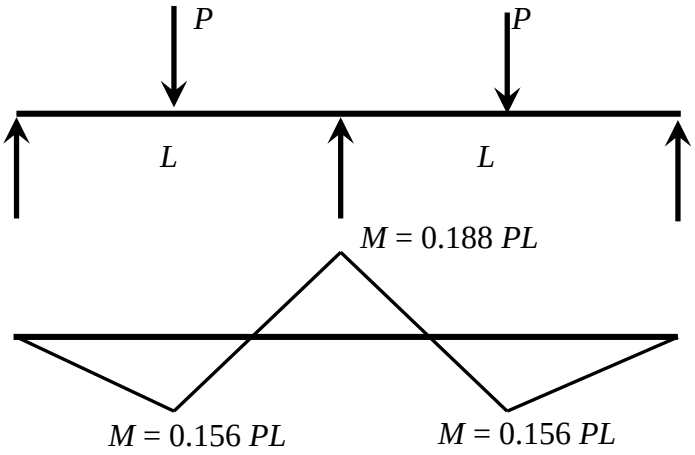

FIGURE 3–7. Elastic bending moment diagram

CHAPTER FOUR

RESULTS AND DISCUSSIONS

In this chapter the material properties of SFRC using compression strength test and splitting strength test results were presented and discussed. Flexural response of each SFRC type was evaluated by deriving the moment-curvature relations and developing a theoretical moment-rotation model that represents the rotational behavior at the plastic hinges.

The computational results were compared with the derived moment-curvature and moment-rotation model and the possibility of moment redistribution was verified. Also the amount of moment redistribution is related to the rotational values at the hinges. Finally the moment redistribution behavior of SFRC continuous beam was analyzed and presented.

4.1 Compressive Strength Results and Tensile strength Results

4.1.1 Compressive Strength Results

As mentioned in methodology, three cubes of each SFRC mix were tested to acquire a representative compressive material behavior. Table 4.1 summarizes the result obtained from the experiments.

TABLE 4–1. Compressive Strength Result of SFRC at the age of 28th day

S. No.	Volume of fiber	Sample No.	Unit Weight	Peak Load	Compressive Strength	Average
	[%]		[kg/m^3]		[MPa]	[MPa]
1	0	1	2429.33	622.81	27.71	27.69
		2	2499.26	650.41	28.91	
		3	2487.71	595.49	26.48	
		Mean	2472.10	622.90		
2	0.5	1	2417.48	753.27	33.48	35.10
		2	2470.81	808.11	35.92	
		3	2424.29	807.58	35.90	
		Mean	2437.53	789.65		
3	0.75	1	2502.22	901.85	40.09	36.18
		2	2485.33	773.76	34.39	
		3	2562.96	766.10	34.05	

		Mean	2516.84	813.90		
4	1.5	1	2474.37	655.62	29.14	26.29
		2	2493.33	557.93	24.81	
		3	2361.48	560.85	24.93	
		Mean	2433.06	591.47		

The compressive strength test result shows that the compressive strength of SFRC is increased for 0.5 % and 0.75 % SFRC by 26.8 % and 30.7 % respectively, however the compressive strength is reduced by 5.3% for 1.5 % SFRC.

TABLE 4–2. Summary of Compressive Strength Results

VF	0%		0.5%		0.75%		1.5%	
MPa	Avg.	CV	Avg.	CV	Avg.	CV	Avg.	CV
σ_{Peak} [MPa]	27.69	3.58	35.10	3.26	36.18	7.66	26.29	7.65
ε_u	0.0045		0.0053		0.0061		0.0069	
E_{Peak} [MPa]	24370.4		26569.4		26869.7		23922.9	

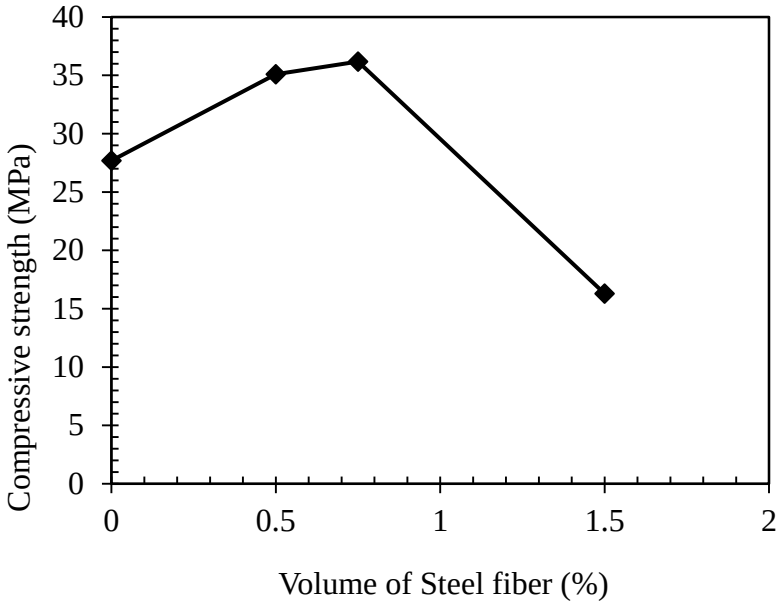

FIGURE 4–1. Compressive Strength of SFRC

TABLE 4–3. Compressive strength of SRFC determined and published by different authors

	Volume of fiber, %		
Authors	0.5	0.75	1.5
(Kovács & Balázs, 2004)	+14		
(Mansur, et al., 1986)	+20	+26	
(Craig, et al., 1986)			-12
(Behbahani, et al., 2012)	+16		
(Bae, et al., 2016)	+3		
(Anusha & kumar, 2015)	+14		

A significant improvement in the post-peak compressive behavior was reported in the published literature. The peak compressive strength of the concrete is marginally increased up to 30 % fiber inclusion in the mix for 0.5% and 0.75 % SFRC as studied by Kovács & Balázs, (2004), Mansur, et al., (1986), (Anusha & kumar, 2015), Bae, et al., (2016) and Behbahani, et al., (2012). But 12% reduction in compressive strength is observed by Craig, et al., (1986) for 1.5 % SFRC.

4.1.2 Compressive Stress-Strain Responses

Figure 4.2 shows the load-displacement response obtained from experimental compressive strength test of SFRC. It is confirmed that the increasing of steel fibers volume increased the displacement of SFRC. The peak load result shows maximum value for 0.5% and 0.75% SFRC.

The compressive stress-strain response of SFRC under compressive given in Figure 4.3 was determined from the load-displacement response of SFRC. The ultimate strain obtained is 0.00455 for 0% SFRC, 0.0053 for 0.5% SFRC, 0.006 for 0.75% SFRC and 0.007 for 1.5% SFRC.

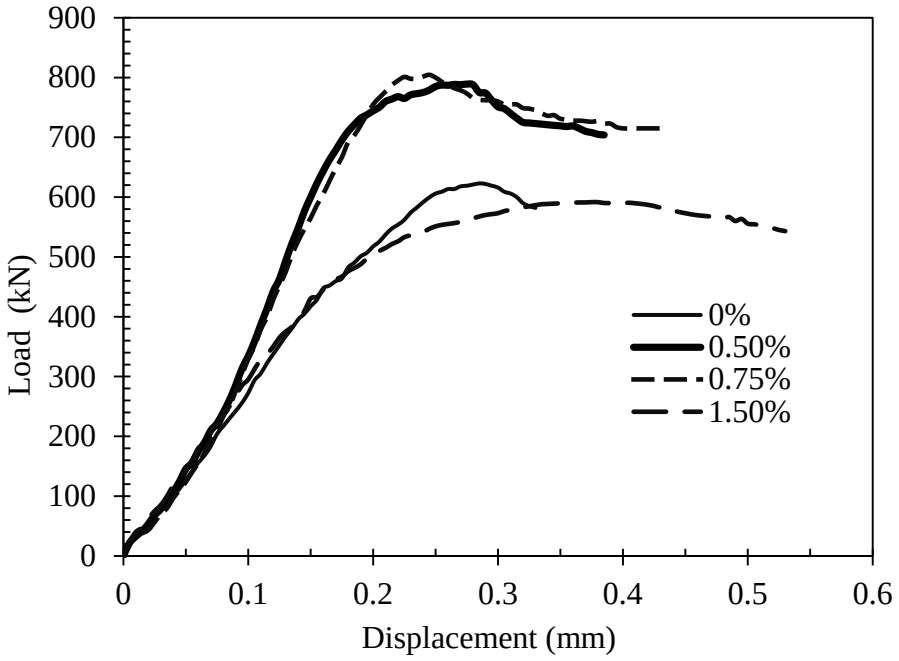

FIGURE 4–2. Load – displacement response of SFRC under compressive

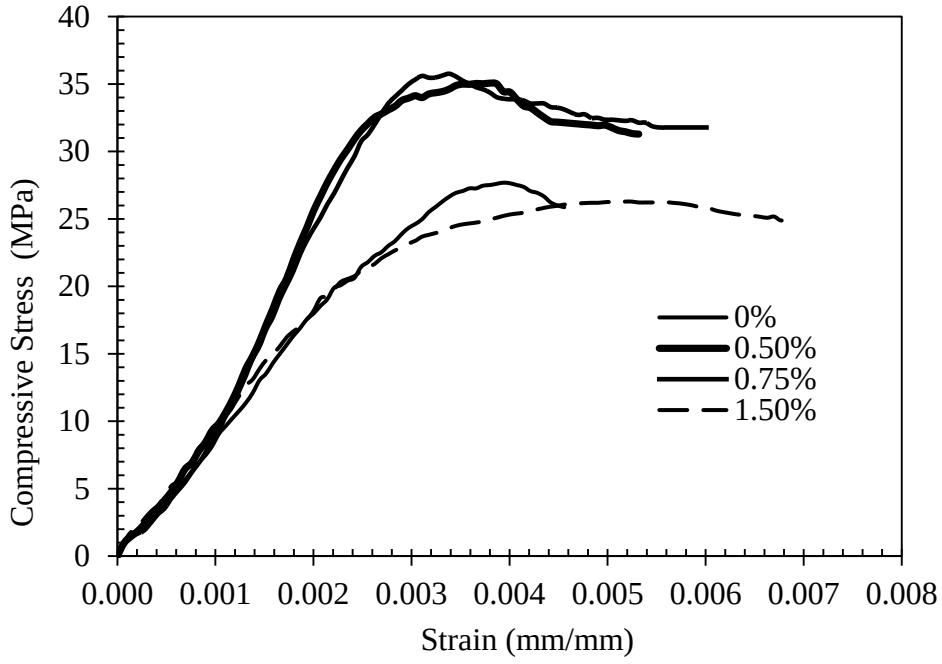

FIGURE 4–3. Compressive stress – strain response of SFRC under compressive

4.2 Tensile behavior (Splitting strength Results) of SFRC

The objective of fibre additions in concrete is often to obtain ductile failure behavior since plain concrete is characterized by its brittle failure behavior in tension. The effect of fiber addition on tensile behavior is clearly shown in table and graph below.

TABLE 4–4. Tensile strength result for SFRC at the age of 28th days

S. No.	Volume of fiber	Sample No.	Unit Weight	Peak Load	Compressive Strength	Average
	[%]		[kg/m^3]		[MPa]	[MPa]
1	0	1	601.69	128.59	4.09	3.93
		2	734.98	131.44	4.18	
		3	655.88	110.11	3.51	
		Mean	668.33	123.38		
2	0.5	1	606.38	140.66	4.45	4.37
		2	591.10	123.25	3.94	
		3	729.57	147.99	4.72	
		Mean	642.35	137.30		
3	0.75	1	605.11	132.60	4.23	4.16
		2	722.48	130.00	4.17	
		3	613.54	127.90	4.08	
		Mean	647.04	130.17		
4	1.5	1	602.72	135.65	4.32	4.03
		2	685.16	118.43	3.78	
		3	731.95	124.56	3.99	
		Mean	673.28	126.21		

The splitting tensile stregnths obatained were 3.93 MPa, 4.37 MPa, 4.16 MPa and 4.03 MPa for 0 % , 0.5% , 0.75% and 1.5 % SFRC respectively. Thus the percentage increased are 11.2 for 0.5%, 5.8 for 0.75% and 2.5 for 1.5% steel fiber addition.

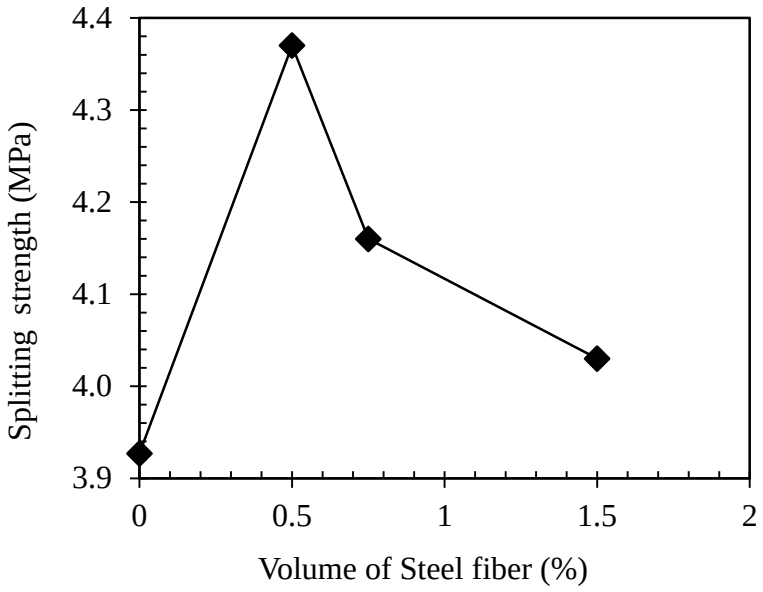

FIGURE 4–4. Tensile strength of SFRC

From Figure 4.3 it is observed that the splitting tensile strength of 0.5% SFRC shows slightly higher increment than 0.75 % and 1.5 % SFRC.

TABLE 4–5. Splitting strength of SRFC determined and published by different authors

	Volume of fiber, %		
Authors	0.5	0.75	1.5
(Kovács & Balázs, 2004)	+67		
(Narayanan & Darwish, 1987)	+28		+93

According to Table 4.5 and Figure 4.3 increments of splitting tensile strength values show considerable differences in the literature due to the different concrete compositions and applied steel fibers. For instance, increment was up to 70% applying 0.5% steel fibers.

Data indicate that splitting tensile strength is very sensitive to the change of the fibre content and the concrete composition but increasing fibre content always produces

significant increment in tensile splitting strength which is approximately proportional to the fibre amount

The difference between the tensile behavior of SFRC and plain concrete is obvious. Due to fiber addition, the tensile strength increased.

4.3 Moment – Curvature Section Analysis for SFRC

The background theory of a sectional analysis is provided to demonstrate the general concept of the moment-curvature relationship. This is followed with the approach developed to consider the material law. The derived moment-curvature relations form the basis of the theoretical models that follow, with the main objective the development of the moment-rotation model. The moment-curvature relations are implemented in finite element analyses of a representative statically indeterminate structure. The theoretical moment – curvature response for all SFRC section is calculated and the result obtained is presented as dimensionless moment, $M_u / f_{ck} BD^2$ with curvature, φ $(\frac{1}{m})$ in figure below.

Figure 4.5 presents a typical set of the moment-curvature responses exhibited by the SFRC beams (for 0 %, 0.5 %, 0.75 % and 1.5 %). The result of moment-curvature responses provide an indication of the sectional ductility.

These moment-curvature response curves are plotted using the constitutive models and corresponding flexural model as discussed in methodology. A similar trend was reported by Singh (2017) and Lini, et al., (1998) for the various test specimens considered in their experimental study.

Figure 4.5 indicate that the section (analyzed with steel fiber of 1.5%) exhibits a slightly higher flexural capacity (15 %) when compared with section having no steel fiber (0 %). Higher flexural capacity is observed with section analyzed with 0.75 % and 0.5 % volume of steel fibers that flexural capacity increased by 57.3% and 52.7% respectively. Mohr (2012) found that the sectional characteristics due to the addition of fibers improved in the range of 58% to 75% for the 0.75% SFRC section.

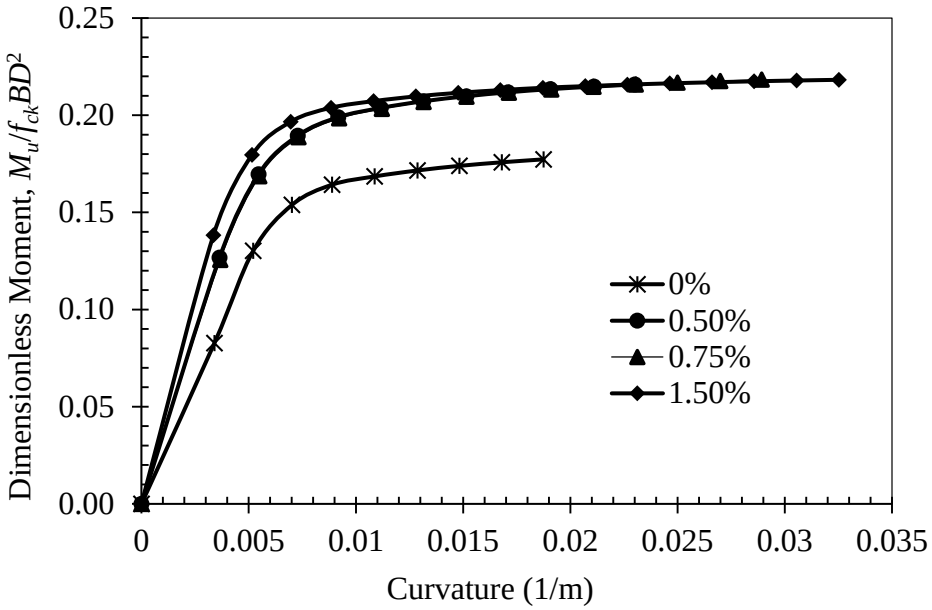

FIGURE 4–5. Moment – curvature response of SFRC

The corresponding value of the section curvature for the 1.5 % SFRC is reduced by 0.4% in comparison to 0 % SFRC, determined corresponding the strain value of 0.004. However, the section curvature for 0.75 % and 0.5 % SFRC slightly increased by 2 %.

Lim, et al., (1987) concluded that the addition of steel fibers is seen to increase the ultimate flexural strength marginally and members having increased amount of steel fibers exhibit less curvature at the same load level.

Singh (2017) studied that the increase in the fiber content enhances the residual tensile strength of the SFRC and, accordingly, there is a slight increase in the section flexural capacity. Nevertheless, the increase in the fiber content bridges the cracks more effectively and it consequently delays the straining of the longitudinal reinforcement present on the tensile face of the beams.

4.4 Moment-rotation response of SFRC

The obtained moment-rotation results are presented in Figure 4.6. The first characteristic that is observed is that the shapes of the curves are similar to that of the moment-curvature relations. This is expected due to the definition of rotation according to the moment-area

theorem, $\theta = \int \frac{M}{EI} dx$. The magnitude of the bending moments was already discussed in the findings of the moment-curvature response.

It is noticed that the deviation of the rotational value at the peak bending moment and plastic rotation capacity has increased with an increase in the fibre volume.

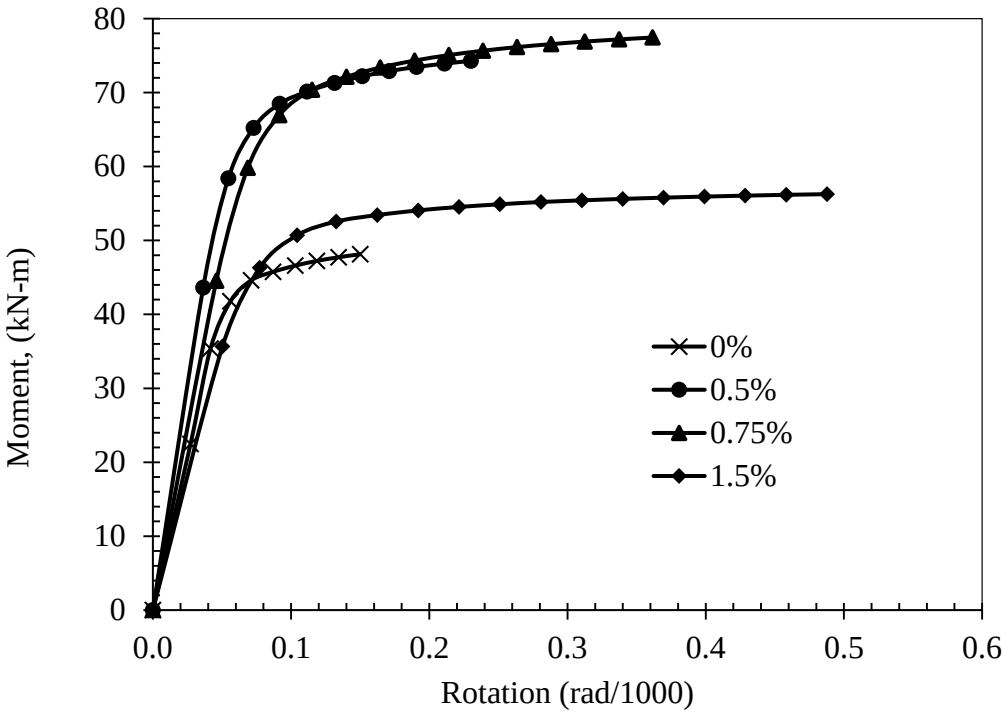

FIGURE 4–6. Moment-rotation response of SFRC

Member ductility ($\Delta\theta$), the amount of plastic rotation experienced at the peak bending moment, is calculated taking 0% SFRC result as the base value and presented in Table 4.6.

TABLE 4–6. Member ductility result

Member Ductility	Volume of Steel fiber			
	0%	0.5%	0.75%	1.5%
$\Delta\theta$ (rad)	0.0015	0.0024	0.0036	0.0049
$\Delta\theta_i / \Delta\theta_{0\%}$	1.0	1.59	2.41	3.25

The member ductility is increased 1.59 times, 2.41 times and 3.25 for 0.5%, 0.75% and 1.5% SFRC member respectively, compared to that of the 0 % SFRC member's rotation capability. The increasing volume of steel fiber increases member ductility.

Mohr (2012) concluded that member ductility increased 1.5 times for 0.75% SFRC by using 0.5% SFRC as the base value. This conclusion is almost the same with the result observed by this study that taking 0.5% SFRC as base value, the member ductility increased 1.52 time for 0.75% and 2.04 times for 1.5% SFRCs respectively.

4.5 Moment Redistribution Behavior of SFRC

This topic presented the calculated elastic bending moment and the result of redistributed moments for modelled continuous beam. Finally the amount of moment redistribution is computed.

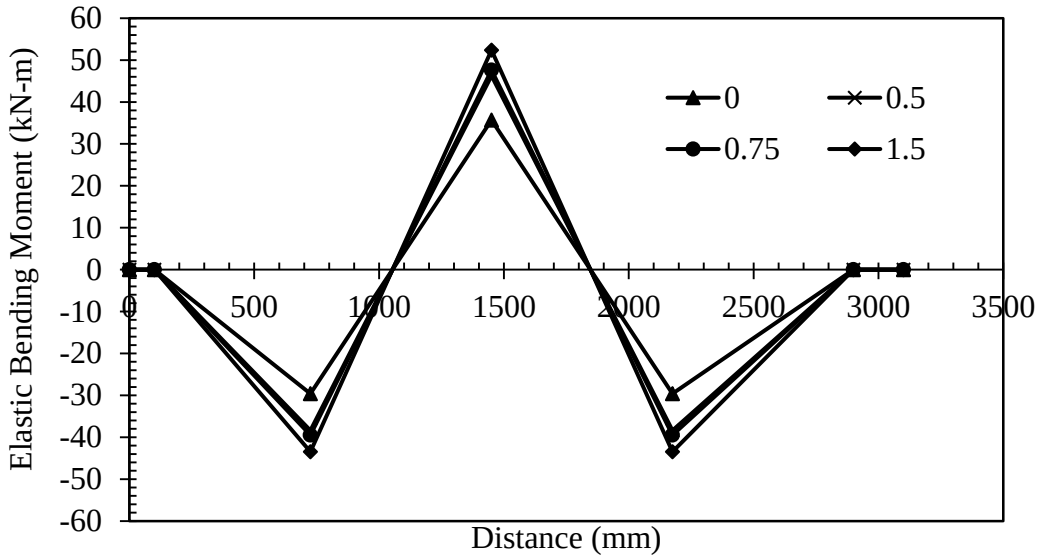

FIGURE 4–7. Elastic bending moment of SFRC

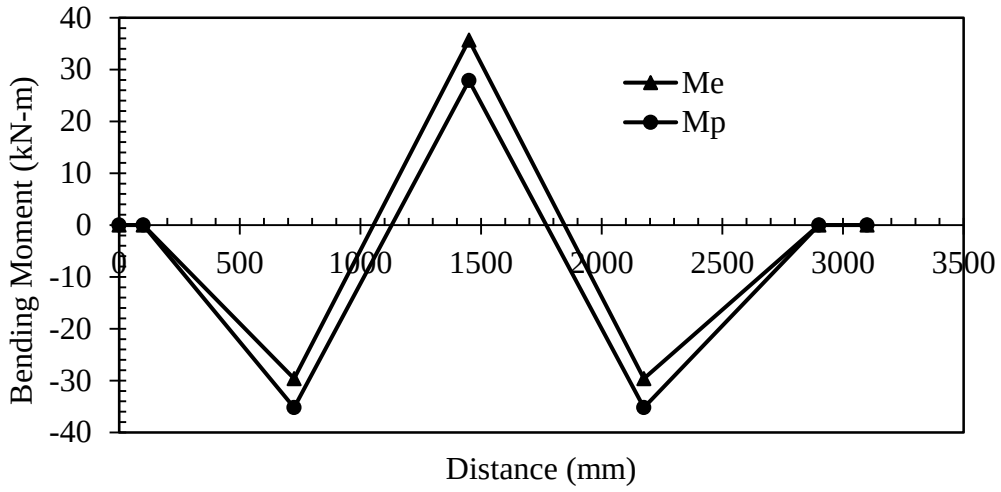

FIGURE 4–8. Elastic and Redistributed bending moments for 0 % SFRC

The results obtained from the analysis of continuous beam using FEA, Abaqus CAE, for SFRC are given as below.

TABLE 4–7. Moment redistribution calculation

Stage	Result	Volume of steel fibers			
		0%	0.5%	0.75%	1.5%
Elastic	$M_{e,\text{span}}$ [kN-m]	29.6	38.4	39.5	43.5
	$M_{e,\text{support}}$ [kN-m]	35.7	46.3	47.6	52.4
Failure	$M_{u,\text{span}}$ [kN-m]	35.2	42.7	43.3	48.2
	$M_{u,\text{support}}$ [kN-m]	27.9	37.5	39.0	45.1
	$P_{\max}$ [kN]	130.9	169.7	174.6	192.1
Moment Redistribution	δ	0.782	0.810	0.819	0.861
	MR [%]	21.8	19	18.1	13.9

From Table 4.7 the amount of moment redistribution obtained are 21.8% for 0%, 19% for 0.5%, 18.1% for 0.75% and 13.9% for 1.5% SFRC. From the values of moment redistribution, a reduction in the amount of moment redistribution is observed with an increase in the fibre volume, which is attributed to the more rapid decrease of the post-peak bending capacity. The maximum amount of moment redistribution (21.9 by percent) is confirmed for 0% SFRC.

According to Mohr (2012) study the reduction of moment redistribution was also observed due to increase of steel fiber contents. The reduction is 14.48 % and 13.05% for 0.5% SFRC and 0.75% SFRC respectively. The final amount of moment redistribution depends on the ability of the first plastic hinge to maintain adequate resistance whilst enabling the mid-span hinges to develop to their maximum capacity. To achieve larger moment redistribution it is beneficial to have a moment-curvature relation with a post-peak behavior which invokes the development of the hinge whilst retaining the necessary structural resistance (Möhr, 2012).

CHAPTER FIVE

CONCLUSION AND RECOMMENDATION

5.1 Conclusion

In this study, material tests are conducted to evaluate the properties of Steel Fiber Reinforced Concrete which was made from adding steel fibers to concrete under compressive strength test and splitting tensile strength test. The moment redistribution behavior is studied by modelling a continuous beam using FEA after the moment-curvature and moment-rotation responses are analyzed.

Analysis of the test results confirmed that the relevant mechanical properties of SFRC, strain at maximum stress, and elastic modulus, at a given strength result improve in proportion to the volume of steel fiber.

Concrete compressive strength is slightly increased by addition of steel fibers. Applying 0.5% and 0.75% of steel fibre 26.8% and 30.7% increment of concrete compressive strength is observed respectively. However, the observed strength increments are not proportional to the increments of fibre contents. According to the results of the cube compressive strength test, it is observed that the cube compressive strength of specimens made from C25 class of concrete with addition of 0.75% by volume of the SF has increased appreciably compared to other specimens with different percentage of steel fibers. However, for 1.5% volume of steel fiber decrease in compressive strengths of 5.3% is observed which might be caused by the increasing porosity of the concrete matrix.

Splitting strength increments are approximately proportional to the applied steel fibre contents up to 1.5 % obtained on cylinders. The increased result for 0.5%, 0.75% and 1.5% SFRCs is 11.2%, 5.8% and 2.5% respectively. The result of splitting tensile strength tests on 1.5% SFRC shows lower value of splitting strength than by 0.75% SFRC.

Ultimate strain is increased from 0.00455 for 0% SFRC to 0.0053 for 0.5%, 0.006 for 0.75% SFRC and 0.007 for 1.5% SFRC by increasing steel fibre contents resulting in a less steep and reasonably flat descending branch of the stress-strain diagram.

The increase of member ductility is found 1.59 times for 0.5% SFRC, 2.41 times for 0.75% SFRC and 3.25 times for 1.5% SFRC beams concretes compared to plain concrete (0% SFRC). With increasing fiber content, mode of failure is changed from brittle to ductile. With the moment-curvature response it is found that the bending capacity increased with an increase in the volume of fibers; and with moment-rotation responses it is found that member ductility increased with an increase in the volume of fibers.

The amount of moment redistribution shows reduction due to increased volume of steel fibers. The MR results are 21.8%, 19%, 18.1% and 13.9% for 0%, 0.5%, 0.75% and 1.5% SFRC respectively. A SFRC member with an increased amount of steel fibers is able to rotate more at the critical sections, but experienced a lower amount of moment redistribution. It is concluded that the amount of moment redistribution computed for SFRCs are less than the ultimate value of moment redistribution, 30% currently prescribed in design codes of ES EN 2015 and ACI for conventionally reinforced structures.

However, up to 13% moment redistribution is allowed for 0.5% up to 1.5% SFRC, but it is not recommended to utilize the prescribed ultimate values in current design codes for the design of steel fibre reinforced concrete structures.

5.2 Recommendation

The research was only conducted with 0, 0.5%, 0.75% and 1.5% waste steel fibers volume. Similar research could be conducted with other volumes of fibers and different type of steel fibers into a high workable steel fiber reinforced concrete which could contribute to the development of a diagram that provides the SFRC's capacity and its ability to redistribute bending moments.

It is recommended for future study to use crack opening, CMOD method for moment-rotation response determination. The effect of important characteristics, such as the span length, cross sectional dimensions, different load applications, etc. and the effect of corrosion should be investigated to determine the influence on the proposed model. Also, the effect that different statically indeterminate structures, e.g. a greater number of span lengths, have on the proposed model, could be investigated.

Future study is recommended to investigate modelling of steel fiber material along with concrete material as matrix in FEA is better approach than modelling using Constitutive material model.

To achieve the probability of getting higher value of moment redistribution it is recommended to use post-peak behavior of the member to generate moment-curvature response that enhances the development of plastic hinge without losing the structural resistance.

REFERENCES

Abaqus/CAE, 6.13. Abaqus Analysis User's Guide, s.l.: s.n.

Abbas, A., Mohsin, S. S. & Costovos, D., n.d. Proceedings of International Conference on Computing in Civil and Building Engineering. s.l., Nottingham University Press.

ACI 318R-14, 2014. Building Code Requirements for Structural Concrete, ACI Committee 318: American Concrete Structure.

ACI 544.4R, 1999. Design Considerations for Steel Fiber Reinforced Concrete, ACI Committee 544: American Concrete Institute.

Anusha, N. & kumar, A., 2015. Experimental study of modulus of elasticity due to change in steel fiber reinforced concrete and size of aggregates. International Journal of Scientific & Engineering Research, 6(7), pp. 465-470.

Bae, B.-I., Choi, H.-K., Lee, B.-S. & Bang, C.-H., 2016. Compressive Behavior and Mechanical Characteristics and Their Application to Stress-Strain Relationship of Steel Fiber-Reinforced Reactive Powder Concrete. Advances in Materials Science and Engineering.

Baker, A., 1956. Ultimate Load Theory Applied to the Design of Reinforced and Prestressed Concrete Frames. London: Concrete Publications Ltd..

Behbahani, H. P., Nematollahi, B. & Farasatpour, M., 2011. Steel Fiber Reinforced Concrete: A Review. ICSECM.

Behbahani, H. P., Nematollahi, B., Sam, A. R. M. & La, F. C., 2012. Flexural Behavior of Steel Fiber Added RC Beams with C30and C50 Classes of Concrete. International Journal of Sustainable Construction Engineering & Technology, 3(1), pp. 54-64.

Chanh, N. V., n.d. Steel Fiber Reinforced Concrete, s.l.: s.n.

Collins, M. P., Mitchell, D. & MacGregor, J. G., 1993. Structural design considerations for high-strength concrete. Concrete International, 15(5), pp. 27-34.

Corley, W., 1966. Rotational Capacity of Reinforced Concrete Beams. Journal of Structural Division, Volume 92, pp. 121-146.

Craig, R. et al., 1986. Fiber Reinforced Beams in Torsion. ACI Journal, pp. 934-942.

Dahake, A. & Charkha, K. S., 2016. Effect of Steel Fibers on Strength of Concrete. Journal of Engineering, Science & Management Education, 9(I), pp. 45-51.

ES EN, 1., 2015. Design of Concrete Structures, Addis Ababa: s.n.

Haskett, M., Oehlers, D. J. & Ali, M. M., 2010. Design for Moment Redistribution in RC Beams Retrofitted with Steel Plates. Advances in Structural Engineering, 13(2).

Hassan, B. & Reza, R. H., 2013. Reliability Analysis of Moment Redistribution in Reinforced Concrete Beams. Magazine of Concrete Research, 65(13), pp. 769-779.

Islam, M. M. et al., 2014. Finite Element Analysis of Steel Fiber Reinforced Concrete (SFRC). Bangladesh, Elsevier Ltd..

Kmiecik, P. & Kaminski, M., 2011. Modelling of reinforced concrete structures and composite structures with concrete strength degradation taken into consideration. Archives of Civil and Mechanical Engineering, XI(3), pp. 623-636.

Kooiman, A. G., 2000. Modelling Steel FIber Reinforced Concrete for Structural Design. Rotterdam: Optima Grafische Communicatie.

Kovács, I. & Balázs, G. L., 2004. Structural Performance of Steel Fibre Reinforced Concrete. Budapest,Hungary, Budapest University of Technology and Economics.

Kwak, H.-G. & Kim, S.-P., 2002. Nonlinear analysis of RC beams based on Moment–Curvature Relation. Computers and Structures , Volume 80, pp. 615-628.

Lee, S.-C., Oh, J.-H. & Cho, J.-Y., 2015. Compressive Behavior of Fiber-Reinforced Concrete with End-Hooked Steel Fibers. Materials, Volume 8, pp. 1442-1458.

Liu, I., Oehlers, D. & Seracino, R., 2006. Moment redistribution in FRP and steel-plated reinforced concrete beams. Journal of composites for construction, 10(2), pp. 115-124.

Mansur, M., Ong, K. & and Paramasivam, P., 1986. Shear Strength of Fibrous Concrete Beams Without Stirrups. Journal of Structural Engineering, 112(9), pp. 2066-2079.

Mattock, A. H., 1967. Rotational Capacity of Reinforced Concrete Beams. Journal of Structural Division, Volume 93, pp. 519-522.

Mitu, S. M., n.d. Finite Element Modeling, Analysis and Validation of the Flexural Capacity of RC Beams Made of SFRC, Bangladesh: s.n.

Möhr, A. W., 2012. Moment Redistribution Behavior of SFRC Members with varying Fibre Content, s.l.: s.n.

Narayanan, R. & Darwish, I., 1987. Use of Steel Fibers as Shear Reinforcement. ACI Structural Journal, pp. 216-227.

Oehlers, D., 2006. Ductility of FRP plated flexural members. Cement & Concrete Composites, Volume 28, pp. 898-905.

Padmarajaiah, S. & Ramaswamy, A., 2002. A finite element assessment of flexural strength of prestressed concrete beams with fiber reinforcement. Cement and Concrete Composites, 24(10), pp. 229-241.

Park, R. & Paulay, T., 1974. Reinforced Concrte Structures. s.l.:John Wiley and Sons.

Salehian, H. R., Barros, J. A. & Taheri, M., 2009. A Design-Based on Approach to Estimate the Moment- Curvature Relationship of Fiber Reinforced Elements Failing in Bending, s.l.: s.n.

Sawyer, H. A., 1964. Design of Concrete Frames for Two Failure States. Miami, s.n.

Scott, R. H. & Whittle, R. T., 2005. Moment Redistribution Effects in Beams. Magazine of Concrete Research, 57(1).

Singh, H., 2017. Steel Fiber Reinforced Concrete Behavior, Modelling and Design. Singabore: Springer Nature.

Tejchman, J. & Kozicki, J., 2010. Experimental and Theoretical Investigations of Steel-Fibrous Concrete. s.l.:Springer-Verlag Berlin Heidelberg.

Tlemat, H., Pilakoutas, K. & Neocleous, K., 2006. Modelling of SFRC using inverse Finite Element Analysis. Materials and Structures, Issue 36, pp. 221-233.

Varghese, P., 2005. Advanced Reinforced Concrete Design. 4th ed. New Delhi: Prentice-Hall of India.

Vasiliev, A. V. et al., 2017. Savings of reinforcement in concrete continuous beam in calculation with Redistribution of Moments. s.l., IOP Conference Series: Earth and Environmental Science.

Wafa, F. F., 1990. Properties and Applications of Fiber Reinforced Concrete. JKAU, Volume 2, pp. 49-63.

APPENDIX

APPENDIX A

STEEL FIBER REINFORCED CONCRTE MATERIAL PROPERTIES AND MIX DESIGN

A1. Fine Aggregate Physical Properties

1.1 Silt Content

Silt content is a fine material which is less than 150 micron. It was unstable in the presence of water. Excessive quantity of silt, not only reduces the bonding of cement and fine aggregates but also affects the strength and durability of work.

1.2 Moisture Content

The objective was to determine moisture content. The procedure followed for the determination of moisture content in fine aggregates was started by measuring of 500g of sand (*A*), then the sample was dried for 24 hours in oven dry. After removal of the sample from oven weigh the sample (*B*) and finally calculation of moisture in sand has done using the following calculation.

$$Moisture\ Content(\%) = \frac{(A-B)}{B}(100)$$

Where, *A* is weight of original Sample (g), *B* is weight of oven dry (g)

TABLE A–1. Determination of Moisture Content for Fine aggregate

S. No.	Description	Sample No.		
		1	2	3
1	A	500	500	500
2	B	494.46	494.27	494.51
3	Moisture Content (%)	1.12	1.16	1.11
	Average	1.13		

1.3 Sieve Analysis for Fine aggregate

The objective of this test was to determine fineness modulus. The procedure started by preparing 2 kg fine aggregate sample. Then the Standard sieves were arranged in descending order with the largest sieve on top. Pour the sample in the top sieve on mechanical shaker. Then switch on the machine and shaking of sieves has done for at least 10-15 minutes. After sieving, the sample weights retained on each sieve has recorded. Then finding the cumulative weight retained has done and given in figure below.

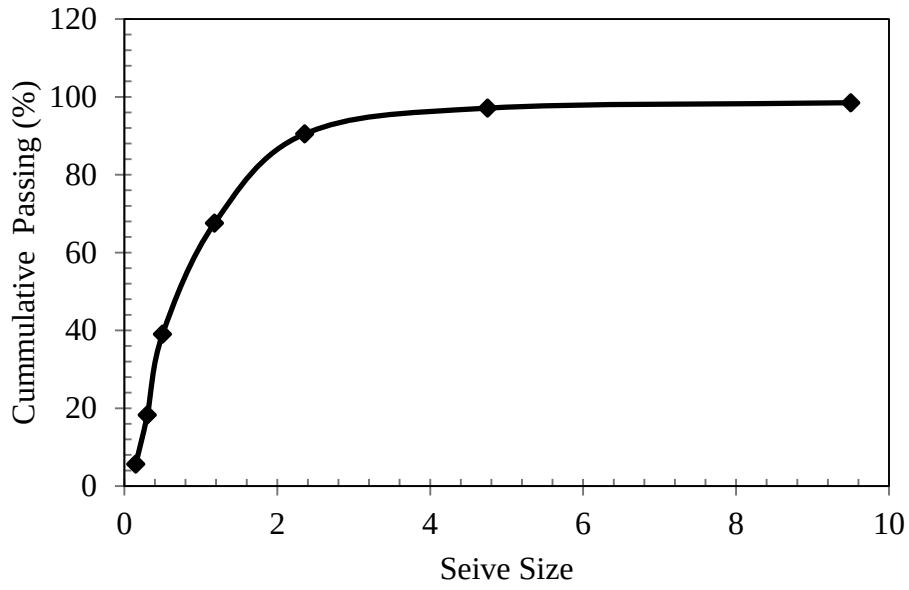

FIGURE A–1. Cumulative % passing versus sieve size

Finally the cumulative percentage retained on each sieves has been determined and all cumulative percentage values divided by 100 generate value for fineness modulus.

$$F.M(\%) = \frac{\sum Cummulative\ Coarser(\%)}{100} \tag{4.1}$$

1.4 Specific Gravity of Fine Aggregate

The aim was to determine bulk and apparent specific gravity of sand and absorption of sand. The procedures are, first, 500g of sample sand, water, pycnometer and balance were prepared. Secondly, poring 500g sand in pycnometer and fill with water to 90% of the capacity, rolling and agitating the pycnometer to eliminate air bubbles have processed. Thirdly filling the water to full level of pycnometer capacity and finally weigh the total weight of the pycnometer, sample, and water together. Therefore from experiment the following results were obtained.

$C = 1838.0\,g, W = 535\,g$, where $C =$ Weight of pycnometer filled with sample and water and $W =$ Weight of the empty pycnometer.

Fourthly fine aggregate was removed from the pycnometer, dry to constant weight at a temperature of 105±5° in oven for 24hrs and after removal of fine aggregates from oven cool in air at room temperature and measurement have done. Lastly the weights of pycnometer filled to its calibration capacity with water were determined. Results obtained are as follows,

$A = 488.0\,g$, $B = 1555\,g$, where $A =$ weight of oven dry sample in air and $B =$ Weight of flask filled with water.

Computation:

$$Bulk\ Specific\ Gravity = \frac{A}{(B + 500 - C)} = 2.249$$

$$Bulk\ SSD\ Specific\ Gravity = \frac{500}{(B + 500 - C)} = 2.304$$

$$Apparent\ Specific\ Gravity = \frac{A}{(A + B - C)} = 2.38$$

$$Absorption\ (\%) = \left(\frac{500 - A}{A}\right) \times 100 = 2.459$$

1.5 Unit Weight of Fine Aggregate

Unit weights was used to define weight of a given volume of graded aggregate. The overall procedure includes filling 1/3, 2/3 and full level of cylindrical metal and 25 times random compaction have done. Finally, the net weights of sand measurement have recorded and unit weight of fine aggregate is determined.

$$Unit\ Weight = \frac{M}{V} \tag{4.2}$$

Where, M is mass of sample (kg) and V is Volume of Cylindrical Metal (kg/m^3)

TABLE A–2. Unit weight of fine aggregate

S. No.	Description	Sample No.		
		1	2	3
1	Mass (kg)	8.697	8.645	8.748
2	Mass of Cylindrical Metal (kg)	1.054	1.054	1.054
3	Net Mass of Sand (kg)	7.643	7.591	7.694
4	Volume of Cylindrical Metal (m^3)	0.005	0.005	0.005
5	Unit Weight (kg/m^3)	1528.6	1518.2	1538.8
	Average	1528.5		

A2. Course Aggregate Physical Properties

2.1 Specific gravity and Absorption test

The test was used to calculate the specific gravity of a coarse aggregate sample by determining the ratio of the weight of a given volume of aggregate to the weight of an equal volume of water and surface absorption capacity.

The coarse aggregate specific gravity test measures coarse aggregate weight under three different sample conditions:

- Oven-dry (no water in sample).
- Saturated surface-dry (SSD, water fills the aggregate pores).
- Submerged in water (underwater).

Using these three weights and their relationships, a sample's apparent specific gravity, bulk specific gravity and bulk SSD specific gravity as well as absorption can be calculated.

Procedures:

i. Obtain a sample of coarse aggregate material retained on the No. 4 (4.75 mm) sieve. This sample size is based on nominal maximum aggregate size. Sample size is 2000 g.

ii. Immerse the aggregate in water at room temperature for a period of 15 to 19 hours(Soaking the aggregate)

iii. Dry the sample to a saturated surface dry (SSD) condition. Rolling up the aggregate into the towel and then shaking and rolling the aggregate from side to side is usually effective in reducing the sample to a SSD condition.

iv. Place the entire sample in a basket and weigh it underwater.

v. Remove the aggregate from the water and dry it until it maintains a constant mass. This indicates that all the water has left the sample. Drying should occur in an oven regulated at 230°F (110°C).

Parameters Measured

1. Coarse aggregate bulk specific gravity.
2. Coarse aggregate bulk SSD specific gravity.
3. Coarse aggregate apparent specific gravity.
4. Coarse aggregate absorption.

$$\text{Bulk Specific Gravity} = G_{sb} = \frac{A}{(B-C)}$$

$$\text{Bulk SSD Specific Gravity} = \frac{B}{(B-C)}$$

$$\text{Apparent Specific Gravity} = G_{sa} = \frac{A}{(A-C)}$$

$$\text{Absorption (\%)} = G_{sa} = \left(\frac{B-A}{A}\right)\times 100$$

Where, A is mass of oven-dry sample in air (g), B is mass of SSD sample in air (g) and C is mass of SSD sample in water (g)

TABLE A–3. Coarse aggregate specific gravity and absorption

S. No.	Description	Sample No.			Average
		1	2	3	
1	C (kg)	1.3	1.31	1.295	1.302
2	B (kg)	2	2	2	2
3	A (kg)	1.980	1.979	1.982	1.980
4	G_{sb}	2.828	2.867	2.811	2.836
5	*SSD* G_{sb}	2.857	2.898	2.837	2.864
6	G_{sa}	2.913	2.960	2.885	2.919
7	Absorption (%)	1.04	1.09	0.91	1.01

2.2 Sieve Analysis

The objective was to get gradation or relative particle size distribution of coarse aggregate by series of square or round opening sieve and also to determine the fineness modulus of aggregate. The retained value of aggregates on each different sieve sizes are given on figure below. The procedures are weighing 10 kg coarse aggregate, putting it on the top of series of sieve (on the largest sieve size) and shaking for a period of 15 minutes by electrical shaker and after 15 minutes measuring each retained mass on each sieve size have done.

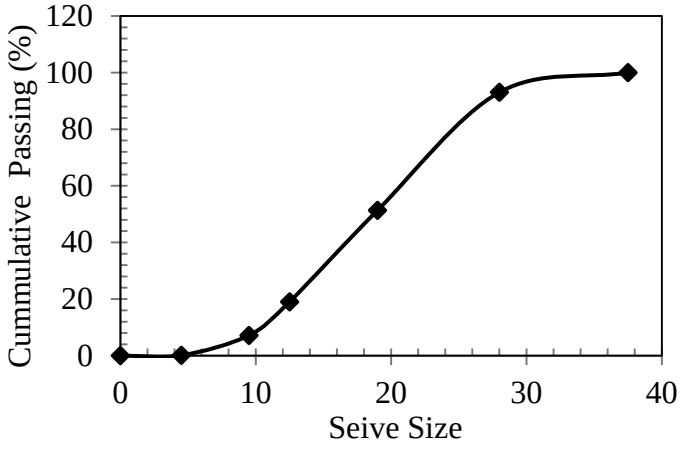

FIGURE A–2. Coarse aggregate particle size distribution curve

2.3 Moisture Content

The procedure for the determination of moisture content in coarse aggregate includes weighing 2000g of coarse aggregate (*A*), oven dry for 24hrs, after removal of the sample after a day weighing the sample (*B*) and finally calculation of moisture in coarse aggregate have determined based on the following calculation.

$$\text{Moisture Content}(\%) = \left(\frac{A-B}{B}\right)\times 100 \tag{4.3}$$

TABLE A–4. Moisture content for coarse aggregate

S. No.	Description	Sample No.		
		1	2	3
1	A	2000	2000	2000
2	B	1978	1980	1982.5
3	Moisture Content (%)	1.11	1.01	0.882
	Average	1.00		

Where, *A* is weight of original Sample (g), *B* is weight of oven dry (g)

2.4 Unit Weight

The unit weight was simply measured by filling a container of known volume and weighing it. Three samples have taken for the determination of unit weight of coarse aggregate.

TABLE A–5. Unit weight for coarse aggregate

S. No.	Description	Sample No.		
		1	2	3
1	Mass (kg)	18.460	18.375	18.350
2	Mass of Cylindrical Metal (kg)	1.695	1.695	1.695
3	Net Mass of Sand (kg)	16.765	16.68	16.655
4	Volume of Cylindrical Metal (m^3)	0.01	0.01	0.01
5	Unit Weight (kg/m^3)	1676.5	1668	1665.5
	Average	1670.0		

A3. ACI 211.1 Mix design

The ACI Standard 211.1-91 is a "*Standard Practice for Selecting Proportions for Normal, Heavyweight, and Mass Concrete*". The procedure is as follows:

Step 1. Choice of slump. If slump is not specified, a value appropriate for the work can be selected from Table 6.3.1(Table A1.5.3.1).

TABLE A–6. Recommended slumps for various types of construction

Types of construction	Slump, mm	
	Maximum*	Minimum
Reinforced foundation walls and footings	75	25
Plain footings, caissons, and substructure walls	75	25
Beams and reinforced walls	100	25
Building columns	100	25
Pavements and slabs	75	25
Mass concrete	75	25

*May be increased 25mm for methods of consolidation other than vibration

Step 2. Choice of maximum size of aggregate

Step 3. Estimation of mixing water and air content

TABLE A–7. Approximate mixing water and air content requirements

TABLE A1.533 — APPROXIMATE MIXING WATER AND AIR CONTENT REQUIREMENTS FOR DIFFERENT SLUMPS AND NOMINAL MAXIMUM SIZES OF AGGREGATES (SI)

Slump, mm	Water, Kg/m³ of concrete for indicated nominal maximum sizes of aggregate							
	9.5*	12.5*	19*	25*	37.5*	50†*	75†‡	150†‡
	Non-air-entrained concrete							
25 to 50	207	199	190	179	166	154	130	113
75 to 100	228	216	205	193	181	169	145	124
150 to 175	243	228	216	202	190	178	160	—
Approximate amount of entrapped air in non-air-entrained concrete, percent	3	2.5	2	1.5	1	0.5	0.3	0.2
	Air-entrained concrete							
25 to 50	181	175	168	160	150	142	122	107
75 to 100	202	193	184	175	165	157	133	119
150 to 175	216	205	197	184	174	166	154	—
Recommended average§ total air content, percent for level of exposure:								
Mild exposure	4.5	4.0	3.5	3.0	2.5	2.0	1.5**††	1.0**††
Moderate exposure	6.0	5.5	5.0	4.5	4.5	4.0	3.5**††	3.0**††
Extreme exposure‡‡	7.5	7.0	6.0	6.0	5.5	5.0	4.5**††	4.0**††

Step 4. Selection of water/cement ratio

The required water/cement ratio is determined by strength, durability and finishability.

TABLE A–8. Relationships between water-cement ratio and compressive strength of concrete

Compressive strength at 28 days, MPa*	Water-cement ratio, by mass	
	Non-air-entrained concrete	Air-entrained concrete
40	0.42	—
35	0.47	0.39
30	0.54	0.45
25	0.61	0.52
20	0.69	0.60
15	0.79	0.70

Step 5. Calculation of cement content

The amount of cement is fixed by the determinations made in Steps 3 and 4 above.

$$Weight\ of\ Cement = \frac{Weight\ of\ water}{w/c} \tag{4.4}$$

Step 6. Estimation of coarse aggregate content

TABLE A–9. Volume of coarse aggregate per unit of volume of concrete

Nominal maximum size of aggregate, mm	Volume of dry-rodded coarse aggregate* per unit volume of concrete for different fineness moduli† of fine aggregate			
	2.40	2.60	2.80	3.00
9.5	0.50	0.48	0.46	0.44
12.5	0.59	0.57	0.55	0.53
19	0.66	0.64	0.62	0.60
25	0.71	0.69	0.67	0.65
37.5	0.75	0.73	0.71	0.69
50	0.78	0.76	0.74	0.72
75	0.82	0.80	0.78	0.76
150	0.87	0.85	0.83	0.81

*Volumes are based on aggregates in dry-rodded condition as described in ASTM C 29.

Step 7. Estimation of Fine Aggregate Content

At the completion of Step 6, all ingredients of the concrete have been estimated except the fine aggregate. Its quantity can be determined by difference if the "absolute volume" displaced by the known ingredients-, (i.e., water, air, cement, and coarse aggregate), is subtracted from the unit volume of concrete to obtain the required volume of fine aggregate.

Step 8. Adjustments for Aggregate Moisture

Step 9. Trial Batch Adjustments

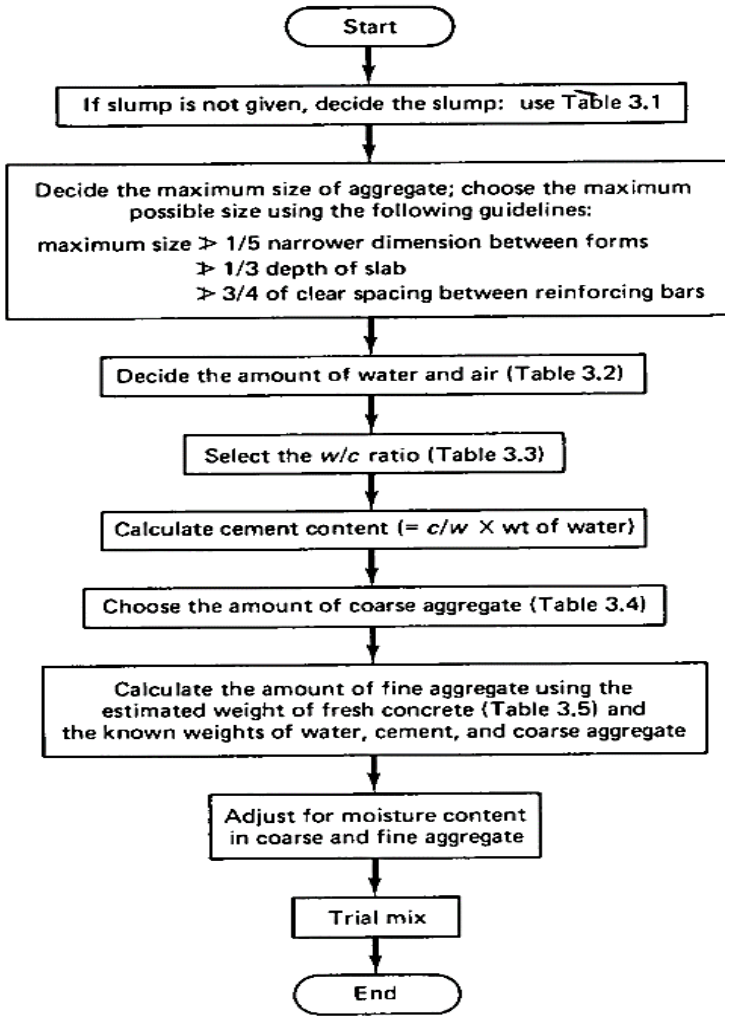

FIGURE A–3. Mix design flow chart

A4. Total Mix Quantity

TABLE A–10. Total Mix quantity

Material	Total Weight (kg/m^3)			
Steel fiber volume	**0 %**	**0.5%**	**0.75%**	**1.5%**
Cement	398.93	398.93	398.93	398.93
Fine Aggregate	761.86	761.86	761.86	761.86
Coarse Aggregate	1140.77	1140.77	1140.77	1140.77
Steel fiber	0	51.93	77.89	155.98
Water	199.43	199.43	199.43	199.43

A5. Illustration of procedures

Fresh concrete

Molded concrete

Curing of concrete

Hardened concrete

FIGURE A–4. Fresh and hardened SFRC

A6. Results of Compressive strength tests

TABLE A–11. Compressive Strength Result for 0 % SFRC at the age of 28th days

S.No.	Dimensions (m)			Weight	Volume	Unit weight	Peak Load	Compressive Strength
	L	*H*	*W*	*kg*	$10^{-3}m^3$	kg/m^3	*kN*	*MPa*
1	0.15	0.15	0.15	8.199	3.375	2429.33	622.81	27.71
2	0.15	0.15	0.15	8.435	3.375	2499.26	650.41	28.91
3	0.15	0.15	0.15	8.396	3.375	2487.71	595.49	26.48
Average				8.343		2472.10	**622.9**	**27.69**

TABLE A–12. Compressive Strength Result for 0.5 % SFRC at the age of 28th days

S.No.	Dimensions (m)			Weight	Volume	Unit weight	Peak Load	Compressive Strength
	L	*H*	*W*	*kg*	$10^{-3}m^3$	kg/m^3	*kN*	*MPa*
1	0.15	0.15	0.15	8.159	3.375	2417.48	753.27	33.48
2	0.15	0.15	0.15	8.339	3.375	2470.81	808.11	35.92
3	0.15	0.15	0.15	8.182	3.375	2424.29	807.58	35.90
Average				8.227		2437.53	**789.65**	**35.10**

TABLE A–13. Compressive Strength Result for 0.75 % SFRC at the age of 28th days

S.No.	Dimensions (m)			Weight	Volume	Unit weight	Peak Load	Compressive Strength
	L	*H*	*W*	*kg*	$10^{-3}m^3$	kg/m^3	*kN*	*MPa*
1	0.15	0.15	0.15	8.445	3.375	2502.22	901.85	40.09
2	0.15	0.15	0.15	8.388	3.375	2485.33	773.76	34.39
3	0.15	0.15	0.15	8.650	3.375	2562.96	766.10	34.05
Average				8.494		2516.84	**813.90**	**36.18**

TABLE A–14. Compressive Strength Result for 1.5 % SFRC at the age of 28th days

S.No.	Dimensions (m)			Weight	Volume	Unit weight	Peak Load	Compressive Strength
	L	*H*	*W*	*kg*	$10^{-3}m^3$	kg/m^3	*kN*	*MPa*
1	0.15	0.15	0.15	8.351	3.375	2474.37	655.62	29.14
2	0.15	0.15	0.15	8.415	3.375	2493.33	557.93	24.81
3	0.15	0.15	0.15	7.970	3.375	2361.48	560.85	24.93
Average				8.250		2433.06	**591.47**	**26.29**

Figure A–5. Failure mechanism of 0.5 % SFRC under compression test

A7. Results of Splitting strength tests

TABLE A–15. Splitting strength result for 0 % SFRC at the age of 28th days

S.No.	Dimensions (m)		Weight	Volume	Unit weight	Peak Load	Tensile Strength
	L	*Dia.*	*kg*	$10^{-3}m^3$	kg/m^3	*kN*	*MPa*
1	0.20	0.10	3.781	6.283	601.69	128.59	4.09
2	0.20	0.10	4.618	6.283	734.98	131.44	4.18
3	0.20	0.10	4.121	6.283	655.88	110.11	3.51
Average			4.199		668.33	**123.38**	**3.93**

TABLE A–16. Splitting strength result for 0.5 % SFRC at the age of 28th days

S.No.	Dimensions (m)		Weight	Volume	Unit weight	Peak Load	Tensile Strength
	L	*Dia.*	*kg*	$10^{-3} m^3$	kg/m^3	*kN*	*MPa*
1	0.20	0.10	3.810	6.283	606.38	140.66	4.45
2	0.20	0.10	3.714	6.283	591.10	123.25	3.94
3	0.20	0.10	4.584	6.283	729.57	147.99	4.72
Average			4.036		642.35	**137.30**	**4.37**

TABLE A–17. Splitting strength result for 0.75 % SFRC at the age of 28th days

S.No.	Dimensions (m)		Weight	Volume	Unit weight	Peak Load	Tensile Strength
	L	*Dia.*	*kg*	$10^{-3} m^3$	kg/m^3	*kN*	*MPa*
1	0.20	0.10	3.802	6.283	605.11	132.60	4.23
2	0.20	0.10	4.540	6.283	722.48	130.00	4.17
3	0.20	0.10	3.855	6.283	613.54	127.90	4.08
Average			4.066		647.04	**130.17**	**4.16**

TABLE A–18. Splitting strength result for 1.5 % SFRC at the age of 28th days

S.No.	Dimensions (m)		Weight	Volume	Unit weight	Peak Load	Tensile Strength
	L	*Dia.*	*kg*	$10^{-3} m^3$	kg/m^3	*kN*	*MPa*
1	0.20	0.10	3.787	6.283	602.72	135.65	4.32
2	0.20	0.10	4.305	6.283	685.16	118.43	3.78
3	0.20	0.10	4.599	6.283	731.95	124.56	3.99
Average			4.230		673.28	**126.21**	**4.03**

FIGURE A–6. Failure mechanism for 0.5 % SFRC under splitting tensile test

APPENDIX B

MOMENT REDISTRIBUTION MODELING AND FEA OUTPUTS OF SFRC

B1. Moment-curvature response

TABLE B–1. Moment-curvature response determination spreadsheet

IBPUT

Section			Concrete			Reinforcement Steel		
B =	150	mm	f_{ck} =	26.29	MPa	f_y =	415	MPa
D =	250	mm	E_c =	26570	MPa	E_s =	200000	MPa
			ε =	0.004		d' =	25	mm
						d =	225	mm
						A_{st} =	402.1	mm^2

OUTPUT

ω =	0.190							
β =	3.901		σ_τ =	102.5	MPa			
γ =	0.870							
ξ =	1	SFRC						
ξ =	0.86	RC						
						Balanced		
h_1/D =	0.941		h_1 =	235.4	mm	$h_{1,b}$ =	225	mm
h_2/D =	0.059		h_2 =	14.64	mm	$h_{2,b}$ =	0	mm
d'/D =	0.100							
D/h_2 =	17.071							

Dimensionless Moment

$M_u/f_{ck}BD^2$ = 0.2125

Moment: M_u = 52.38 kN-m

TABLE B–2. Sample moment-curvature result

0% SFRC		
φ	M	$\frac{M_u}{f_{ck}BD^2}$
0	0	0
0.0034	22.5	0.083
0.0052	35.4	0.130
0.0070	41.8	0.154
0.0089	44.6	0.164
0.0109	45.8	0.168
0.0129	46.6	0.172
0.0148	47.2	0.174
0.0168	47.7	0.176
0.0188	48.1	0.177

0.5% SFRC		
φ	M	$\frac{M_u}{f_{ck}BD^2}$
0	0	0
0.004	43.6	0.127
0.005	58.4	0.170
0.007	65.2	0.190
0.009	68.5	0.199
0.011	70.1	0.204
0.013	71.3	0.207
0.015	72.2	0.210
0.017	72.9	0.212
0.019	73.5	0.213
0.021	73.9	0.215
0.023	74.3	0.216

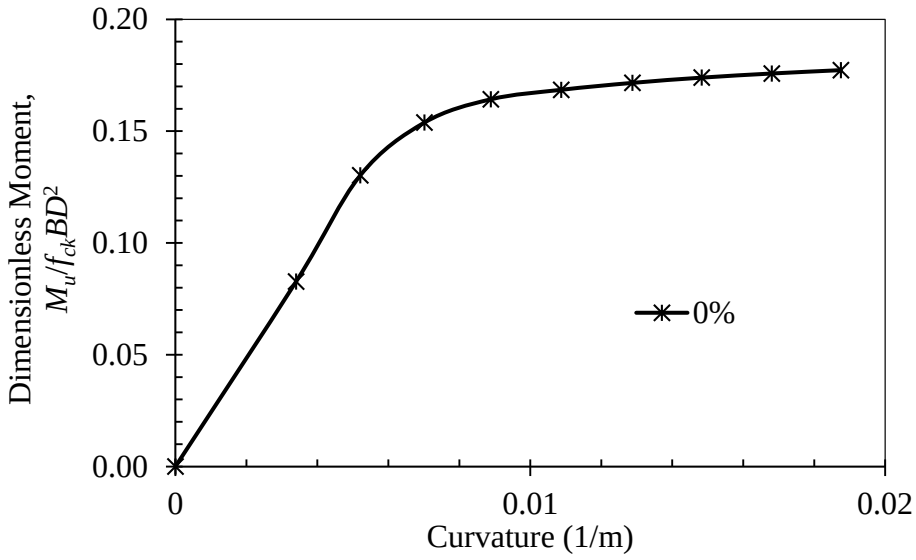

FIGURE B–1. Moment-curvature response of 0% SFRC

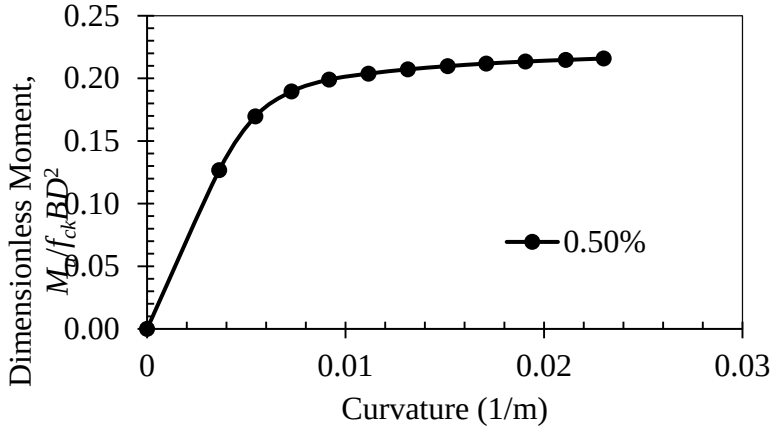

FIGURE B–2. Moment-curvature response of 0.5% SFRC

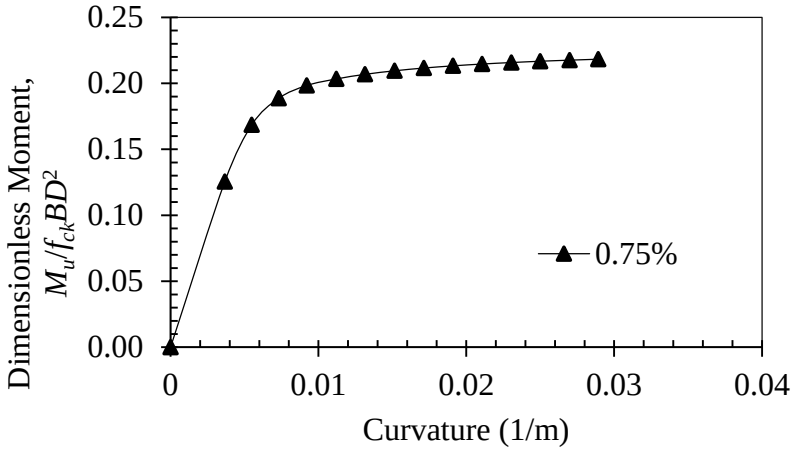

FIGURE B–3. Moment-curvature response of 0.75% SFRC

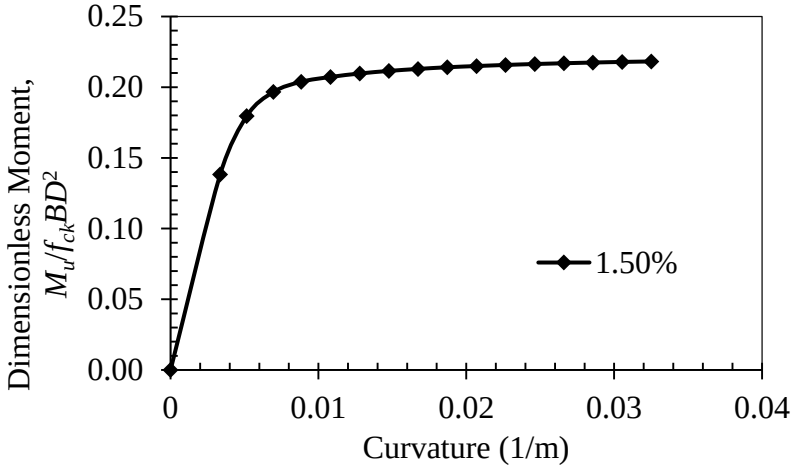

FIGURE B–4. Moment-curvature response of 0.75% SFRC

B2. Moment-rotation response

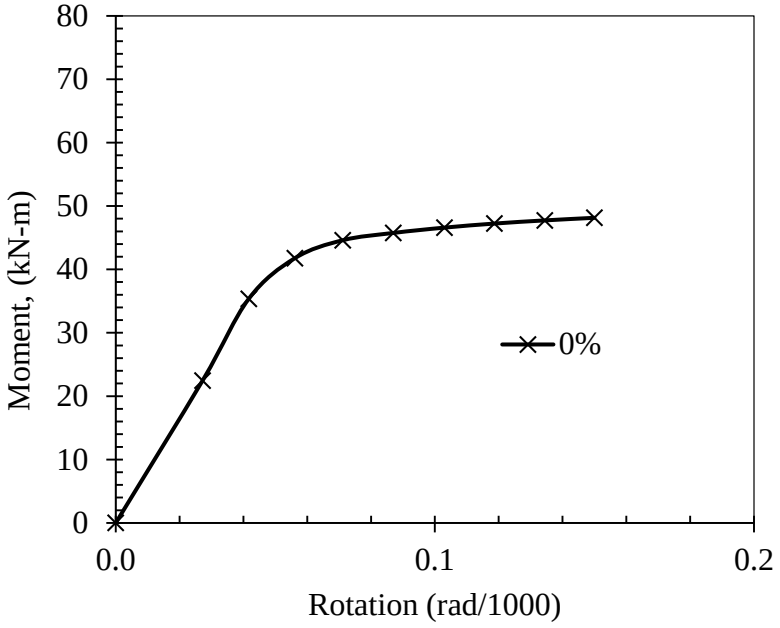

FIGURE B–5. $M-\theta$ response of 0 % SFRC

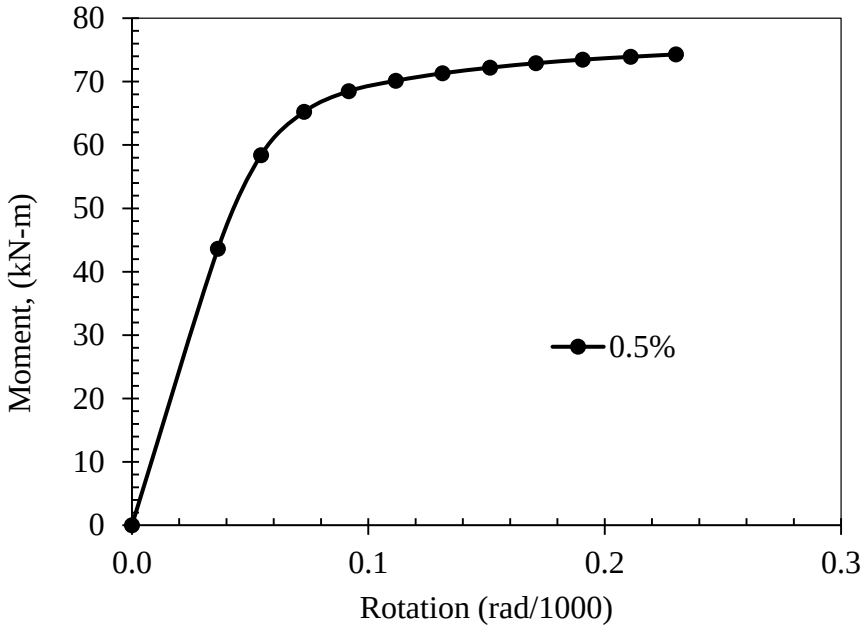

FIGURE B–6. $M-\theta$ response of 0.5 % SFRC

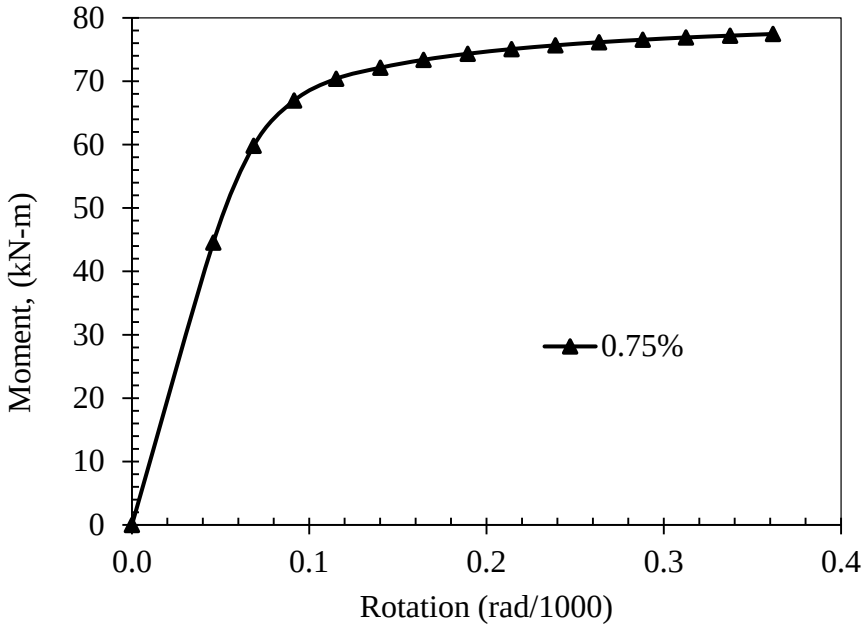

FIGURE B–7. $M-\theta$ response of 0.75 % SFRC

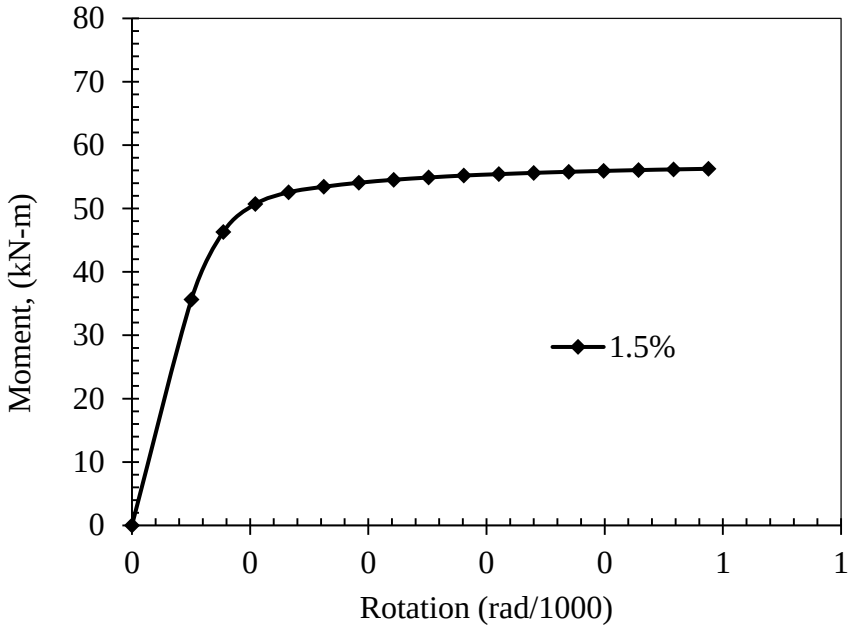

FIGURE B–8. $M-\theta$ response of 1.5 % SFRC

B3. Moment-redistribution model [ABAQUS/CAE]

ABAQUS/CAE Finite element was used for modelling continuous SFRC beam for each steel fiber volumes.

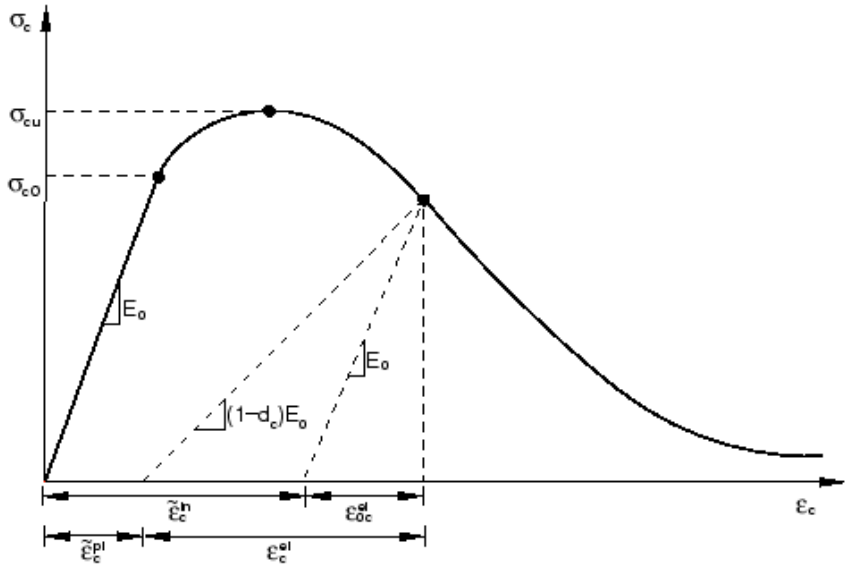

FIGURE B–9. Concrete damaged compressive stress-inelastic strain response (Abaqus/CAE, 6.13)

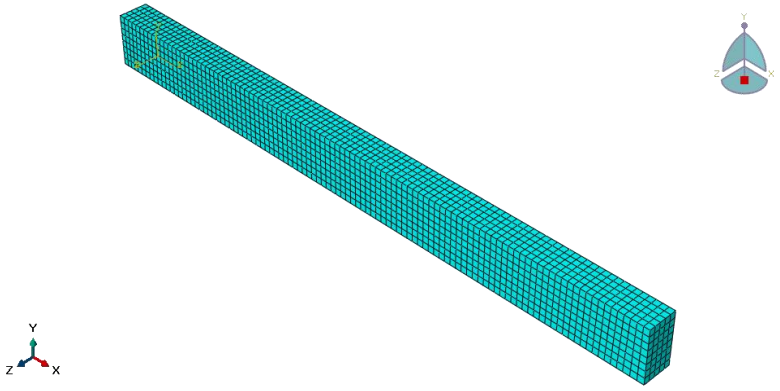

FIGURE B–10. Mesh

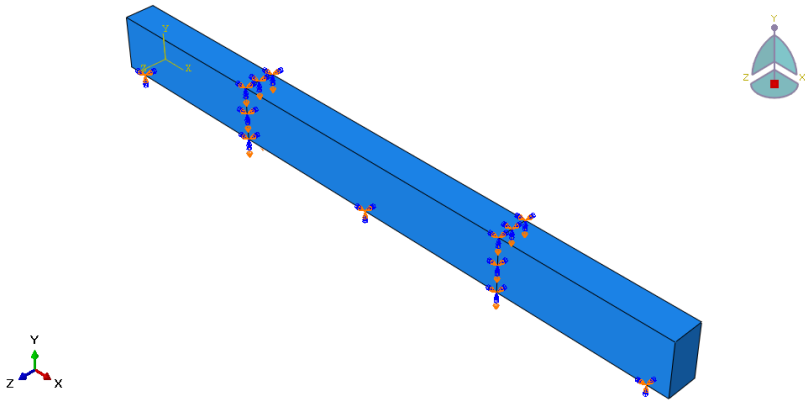

Figure B–11. Boundary conditions

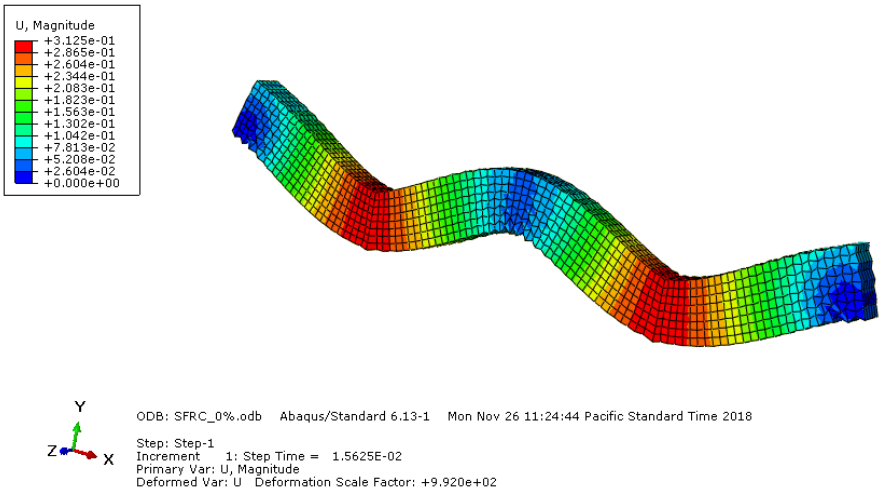

FIGURE B–12. Deformed beam after moment redistributed

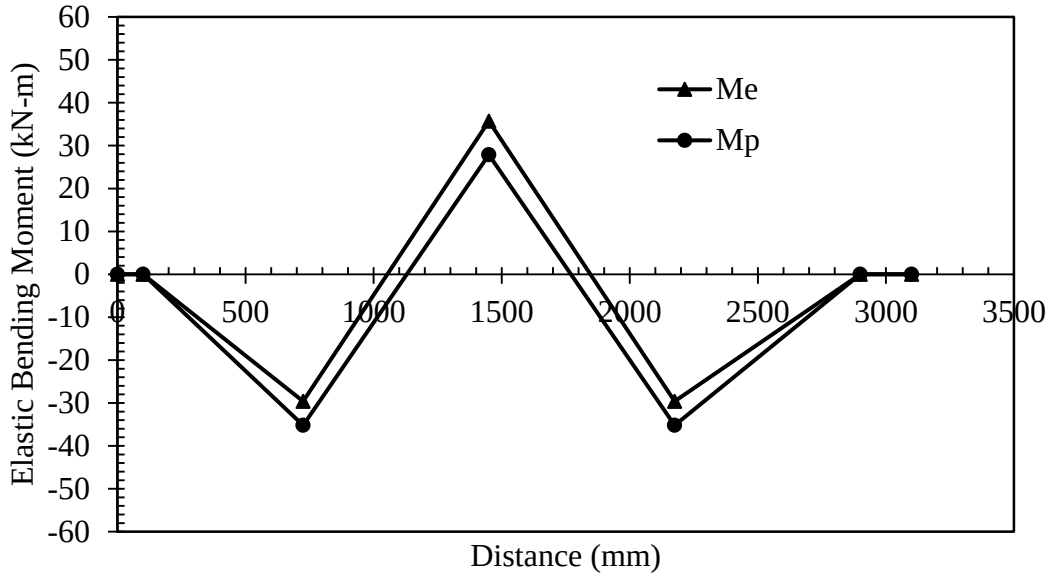

FIGURE B–13. Elastic and Redistributed bending moment for 0 % SFRC

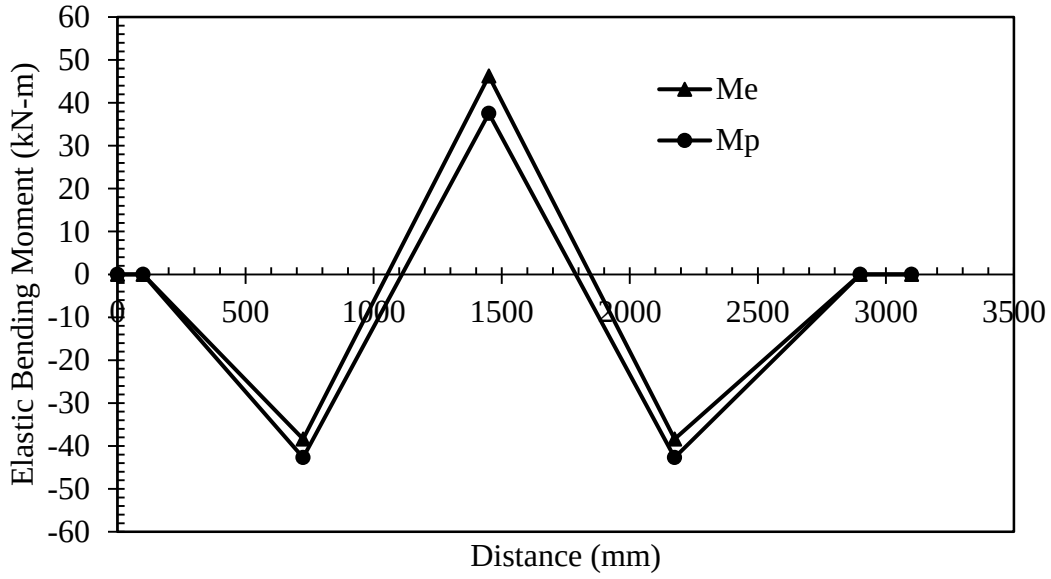

FIGURE B–14. Elastic and Redistributed bending moment for 0.5% SFRC

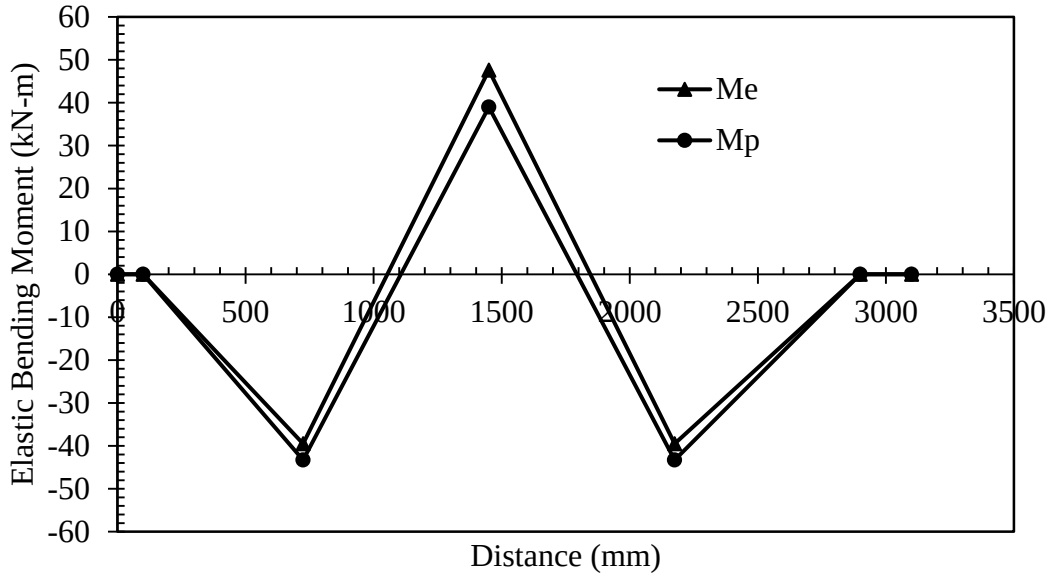

FIGURE B–15. Elastic and Redistributed bending moment for 0.75% SFRC

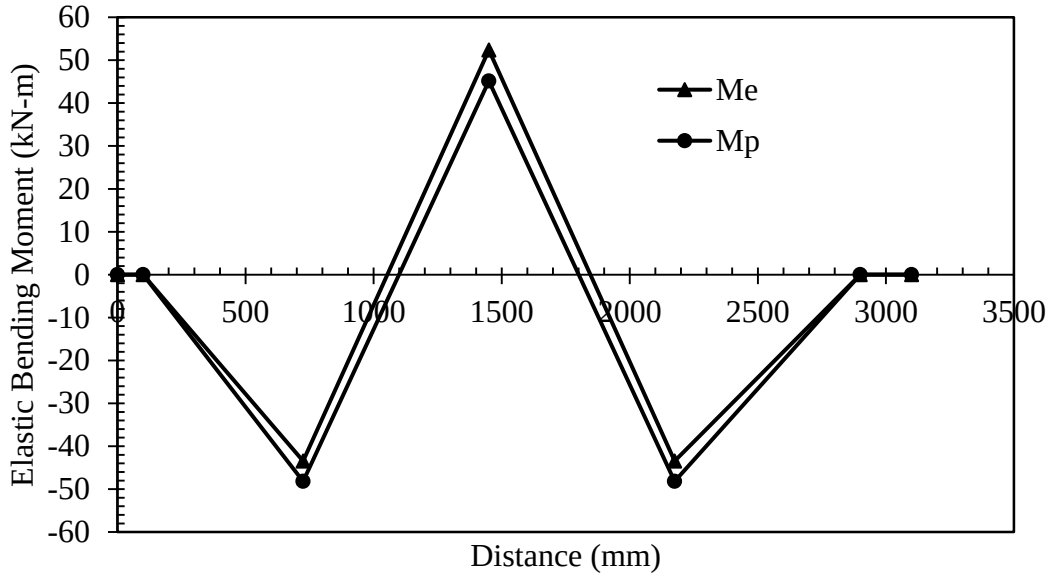

FIGURE B–16. Elastic and Redistributed bending moment for 1.5 % SFRC